ATMOSPHERIC WATER HARVESTING: AN EXPERIMENTAL STUDY OF VIABILITY AND THE INFLUENCE OF SURFACE GEOMETRY, ORIENTATION, AND DRAINAGE

A Thesis

presented to

the Faculty of California Polytechnic State University,

San Luis Obispo

In Partial Fulfillment

of the Requirements for the Degree

Master of Science in Mechanical Engineering

by

Carson Hand

June 2019

COMMITTEE MEMBERSHIP

TITLE: Atmospheric Water Harvesting: An Experimental Study of Viability and the Influence of Surface Geometry, Orientation, and Drainage

AUTHOR: Carson Hand

DATE SUBMITTED: June 2019

COMMITTEE CHAIR: Steffen Peuker, Ph. D.
Professor of Mechanical Engineering

COMMITTEE MEMBER: Kim Shollenberger, Ph. D.
Professor of Mechanical Engineering

COMMITTEE MEMBER: Patrick Lemieux, Ph. D.
Professor of Mechanical Engineering

ABSTRACT

Atmospheric Water Harvesting: An Experimental Study of Viability and the Influence of Surface Geometry, Orientation, and Drainage

Carson Hand

Fresh water collection techniques have gained significant attention due to global dwindling of fresh water resources and recent scares such as the 2011-2017 California drought. This project explores the economic viability of actively harvesting water from fog, and techniques to maximize water collection. Vapor compression and thermoelectric cooling based dehumidifier prototypes are tested in a series of experiments to assess water collection capability in foggy environments, and what parameters can increase that capability. This testing shows an approximate maximum collection rate of 1.25 L/kWh for the vapor compression prototype, and 0.32 L/kWh for the thermoelectric cooling prototype; compared to 315 L/kWh for desalination or 12 L/m^2/day for passive meshes. Exploration of parameters on the thermoelectric cooling prototype show a potential increase in water collection rate of 29% with the addition of a Teflon coating to the collection surface, 15% by clearing the collection surface, and 89% by tilting certain collection surfaces by 60-75°. In combination, these parameters could push active atmospheric water harvesting into economic viability where significant infrastructure investment is not feasible.

Keywords: Vapor compression, thermoelectric cooling, Peltier element, dehumidification, atmospheric water harvesting, fog catching.

TABLE OF CONTENTS

Page

LIST OF TABLES

Table Page

LIST OF FIGURES

Figure Page

Chapter 1: Introduction and Objectives

1.1 Introduction

Potable water collection is becoming an increasing concern as world population rises, and natural fresh water resources are stretched to their limits. This heightened demand opens the door for previously economically unviable methods to be explored and perhaps implemented. This project will explore the viability of actively harvesting water from the air, particularly from coastal fog, and cool high humidity environments. Additionally, this project will focus on ways of maximizing water collection from active water harvesting devices using vapor compression and thermoelectric dehumidification.

1.2 Objectives

The objectives of this project are to determine the viability of active atmospheric water harvesting using vapor-compression and thermo-electric-cooling device prototypes, to discover ways of maximizing the effectiveness of these devices, and to understand the parameters that most impact their performance. Due to its high modularity, this project will primarily use the thermoelectric cooling prototype to explore the optimizing parameters of a particular device configuration. The vapor compression prototype will provide a baseline collection rate on which these parameters can be projected to develop an idea of the capability of a fully optimized device.

Chapter 2: Background

2.1 The Challenge

Water collection and purification is not a new concept. For places around the world where there have been serious water shortages, several different ideas for harvesting usable water have been explored. The most obvious water collection techniques might be trivial, but they are necessary options to consider before water collecting becomes too difficult, expensive, or inefficient. If there is not enough rainfall to support a large body of fresh water, one might turn to groundwater beneath the surface and dig wells to collect the valuable resource. For places like the Atacama Desert in Chile, rainfall is so infrequent that there is no water to harvest at a reachable depth below the surface. The increasing scarcity of fresh water around the world due to climate change and population growth is a persistent problem that will only get worse. The recent California drought is only a local reminder of a much larger problem. New options must be explored in order to help properly prepare for the water shortage inevitability.

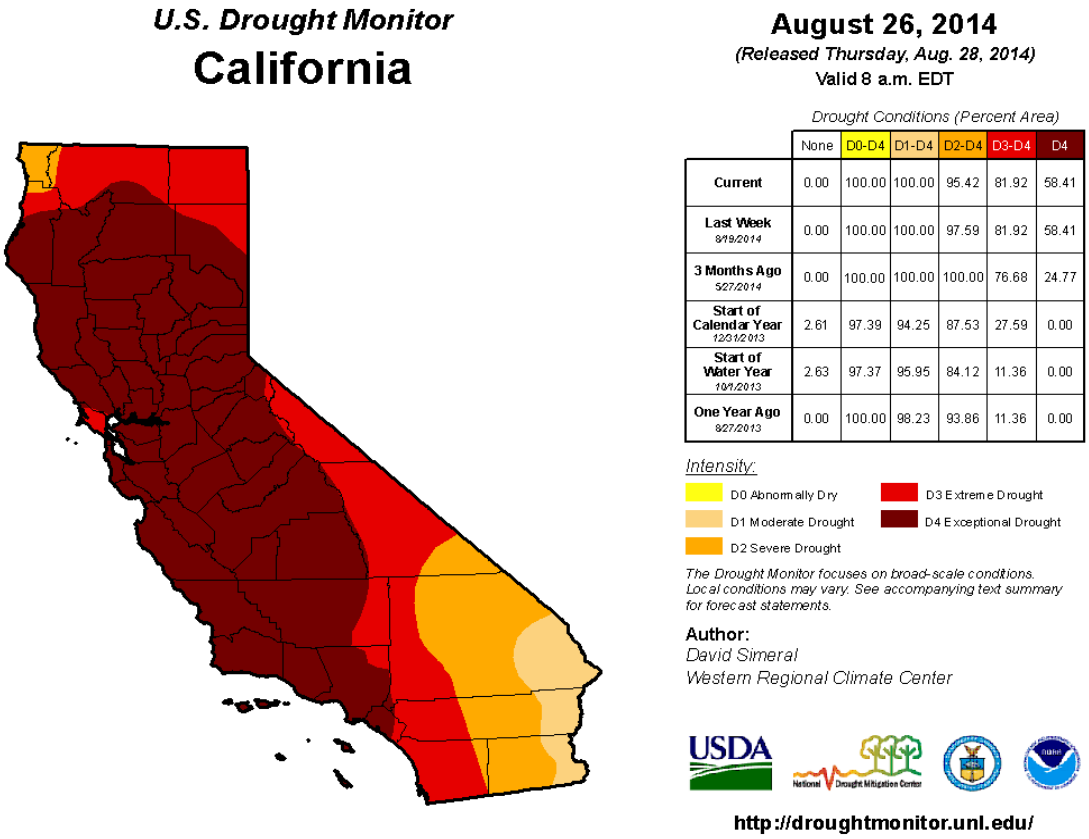

Figure 1. California drought map. (1)

2.2 Alternative Water Sources

2.2.1 Desalination

The earth is covered by 71% water, but only 3% of all water is contained inland and the other 97% is contained by the ocean. Unfortunately, seawater is not drinkable by humans in its natural state because of its high salt content; the extremely salty solution actually draws water out of the body's cells via osmosis, leaving the drinker less hydrated than before. This problem gave birth to a technique of water extraction known as desalination where the salt is extracted to provide drinkable water. There are two primary processes for desalting salt water: membrane and filtration processes

and thermal processes. In the first method, salt water is forced through selectively permeable membranes to filter the salt and other contaminants out of the water. The most common of these methods is reverse osmosis (RO). In the thermal method, salt water is heated to the boiling point and the vapor travels to a collector while leaving behind salt or very salty water known as brine. This process mimics the natural water cycle, but can be performed much more quickly. The most common thermal desalination processes are multi-stage flash distillation (MSF) and multiple-effect distillation (MED). Other desalination processes include electron dialysis (ED), which uses an electric current to move salt ions through a selectively permeable membrane, and electrodeioniation (EDI), which uses ion-exchange methods to separate the salt from the water (2). The figure below shows that reverse osmosis and multi-stage flash distillation account for approximately 86.8% of the installed capacity of desalination plants.

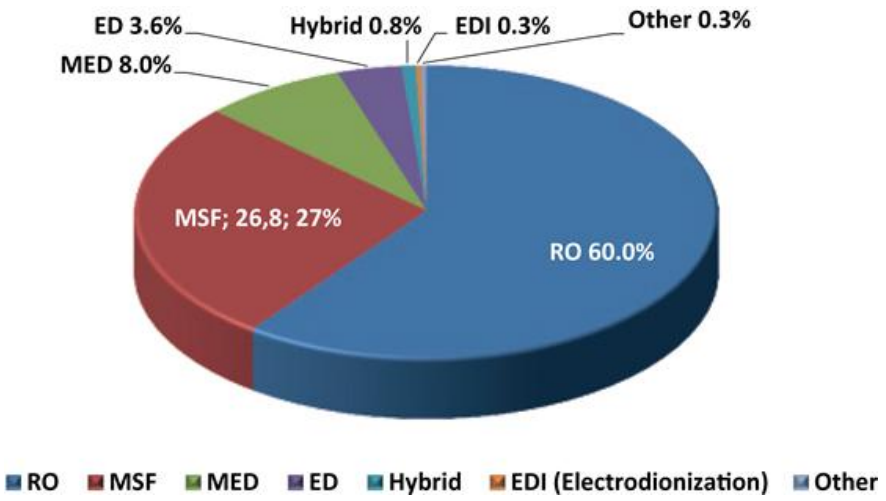

Figure 2. Worldwide desalination capacity by type in 2010. (3)

Diagrams of the two most common desalination processes, multi-stage flash and reverse osmosis, are shown in Figure 3 and Figure 4 respectively.

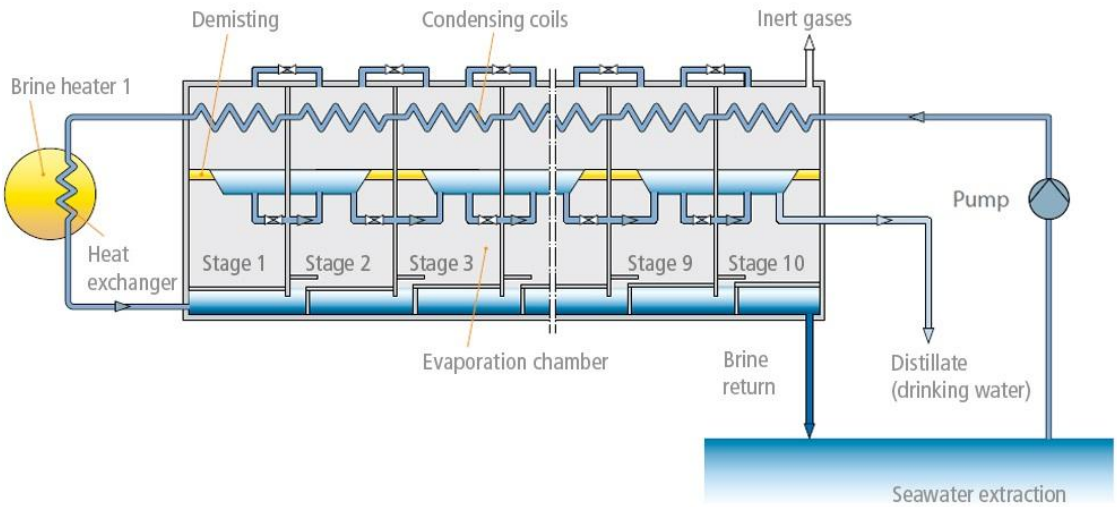

Figure 3. Multi-stage flash desalination process. (4)

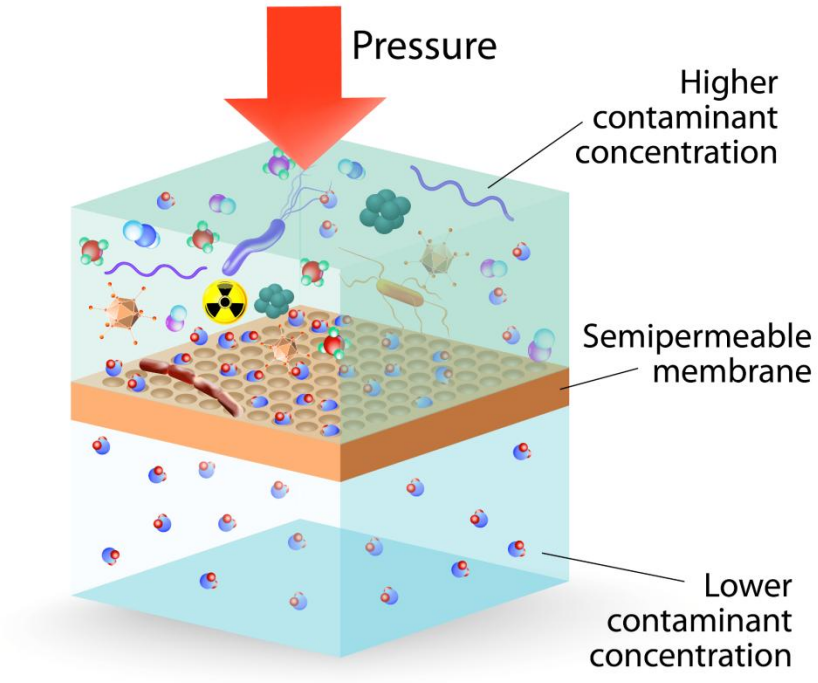

Figure 4. Reverse osmosis process. (5)

Table 1. The first-year cost of the water production for various desalination plants around the world, with the year of the projected cost and the data source. (2)

Facility or Location	US$/kgal (first year)	US$/m³ (first year)	Operational?	Year	Source
Ashkelon, Israel	2.03	0.54	Yes	2002	EDS (2004), Segal (2004), Zhou & Tol (2005)
Ashkelon, Israel	2.00	0.53	Yes	2003	NAS (2004)
Ashkelon, Israel	2.10	0.55	Yes	2004	Wilf & Bartels (2005)
Ashkelon, Israel	2.34	0.62	Yes	2005	Red Herring (2005), Semiat (2006)
Bahamas	5.60	1.48	Yes ?	2003	NAS (2004)
Carlsbad, CA (Poseidon)	2.90	0.77	No	2005	San Diego Daily Transcript (2005)
Dhekelia, Cyprus	4.14	1.09	Yes	1996	Segal (2004)
Dhekelia, Cyprus	5.40	1.43	Yes	2003	NAS (2004)
Eilat, Israel	2.80	0.74	Yes	1997 ?	Wilf & Bartels (2005)
Hamma, Algiers	3.19	0.84	No	2003	EDS (2004), Segal (2004)
Larnaca, Cyprus	2.84	0.75	Yes	2000	Segal (2004)
Larnaca, Cyprus	3.20	0.85	Yes	2003	NAS (2004)
Larnaca, Cyprus	3.23	0.85	Yes	2001 ?	Wilf & Bartels (2005)
Moss Landing, CA (Cal Am)	4.75[1]	1.28[1]	No	2005	MPWMD (2005b)
Moss Landing, CA (Poseidon)	3.63	0.96	No	2005	MPWMD (2005b)
Perth, Australia	3.49	0.92	No	2005	Water Technology (2006)
Singapore	1.75	0.46	Yes	2002	Segal (2004)
Singapore	1.70	0.45	Yes	2003	NAS (2004)
Sydney, Australia	4.21[2]	1.11[2]			
Tampa Bay, FL	Four bids from 1.75 to 2.18	0.46 to 0.58	No	1999	Semiat (2000)
Tampa Bay, FL	2.10	0.55	No	2003	Segal (2004)
Tampa Bay, FL	2.18	0.58	No	2003 ?	Wilf & Bartels (2005)
Tampa Bay, FL	2.49	0.66	No	?	Arroyo (2004)
Trinidad	2.77	0.73	Yes	?	Segal (2004)
Trinidad	2.80	0.74	Yes	2003	NAS (2004)

The first year water costs (US$/$m^3$) shown in Table 1 range from \$0.45/m^3 to \$1.48/m^3 which can provide a useful comparison when evaluating the performance of the active water harvesting design. The best reverse osmosis procedures use approximately 3.2 kWh/m^3 and with the current energy cost in California being approximately \$.1178/kWh for industry (6), the price of reverse osmosis is approximately \$0.38/m^3.

Construction is underway in Carlsbad, CA to build the largest desalination plant in the western hemisphere. This plant will use reverse osmosis, and will be capable of making 190,000 m^3 of freshwater daily. The average cost to turn 1230 m^3 of salt water into fresh water ranges from $800 to $1,400. Water bills would rise $5-7 dollars a month to pay for desalination. The water authority in San Diego will pay $2,014-2,257 per 1230 m^3. Unfortunately, desalination is very energy intensive, requiring approximately 38 Megawatts a day which translates to about double the cost of more common water extraction techniques. Furthermore, desalination is typically only a temporary option for more remote locations until drought conditions lessen naturally or cheaper water sources become available. (7)

2.2.2 Passive Collection: Meshes

Another option currently being researched at MIT and tested in Chile is passive water collection. This method employs large meshes (nets) with material properties and microgeometry that assist in the condensation of water droplets. These meshes are strategically placed (e.g. areas where coastal fog rolls through) to allow fog to pass through and deposit water. Some prototypes can produce approximately 1.9 m^3 per catcher per day. Although this is a significant number it obviously does not compete with the 190,000 m^3 produced by desalination plants daily. Passive fog catching also is dependent on favorable fog and wind conditions which seriously limit its consistency, and it requires a large area for significant production.

In particular, two scientists from MIT investigated the effects of surface

geometry on collection rates of fog. Their datum, Rachel meshes, have been reported to collect anywhere from 0.1-10 L/m^2/day. The variables that were investigated were width of the mesh fibers, shade coefficient, and composition of mesh material. Each of their designs were tested in a controlled-humidity box that kept the relative humidity at 100% and the temperature at 26.4 ± .5 °C. The humid air was propelled by a fan towards the meshes at a speed of 2 m/s. The experiment showed that for fog conditions where the velocity ranged from 1-10 m/s their mesh could collect more efficiently than the Rachel meshes that are the current industry standard. In particular, they predict that in Chile, where passive fog collection is a primary means for obtaining water and the average wind speed is 6 m/s, their meshes may be able to collect up to 12 L/m^2/day. (8)

Figure 5. Passive fog catching meshes. (9)

2.2.3 Active Collection

Active water harvesting methods are uncommon and for the most part underdeveloped, but there are a few designs that exist and are worth mentioning.

The first, shown in Figure 6, is the WMS1000, designed by inventor Marc Parent and sponsored and built by Eole Water. The wind turbine generates all of the power necessary for its compressor-based refrigeration unit. A condenser with a moisture exchange surface 1m wide and 5m long allows the system to collect up to 1500 liters of water a day depending on the weather. (10)

Figure 6. The WMS1000 water collecting wind turbine. (11)

Another concept that utilizes a refrigeration system is the Airdrop, shown below in Figure 7. Air is drawn underground and routed through a series of pipes that rapidly cool it to the temperature of the soil. As it reaches the dew point, water condenses on the pipe and runs into an underground storage area. A pump is then used to move the water through pipes to irrigate the roots of plants. The underground containment of the system also prevents evaporation and runoff losses on the surface. (11)

Figure 7. The Airdrop water collection system in possible agricultural application. (11)

Departing from the use of a refrigeration cycle is the A2WH, shown below in Figure 8. This system uses solar energy to drive a small fan which creates airflow over a salt desiccant that captures the water. Once the salt desiccant is saturated, solar heat bakes a humidity-enriched vapor out of the salt, from which water is condensed and collected at ambient temperature within the device.

Figure 8. The A2WH active moisture harvester. (11)

2.2.4 Dehumidification

One process very similar to the active approaches mentioned above is dehumidification. Dehumidification is the process of removing moisture from the atmosphere in order to keep a comfortable level of humidity. This process is very common in homes that are located in very humid areas and helps to prevent mold from accumulating in dark moist areas. In practice, there are two main types of dehumidifiers, those that employ refrigeration and those that rely on absorption (soaking up water in pore spaces) and adsorption (adherence of a very thin film of water on a surface). Refrigeration dehumidifiers use vapor compression cycles to cool the air to the dew point, at which point water vapor begins to condense. The water is collected in a collection chamber and the dry air is heated to room temperature before exiting the system. Filters are used to maintain cleanliness.

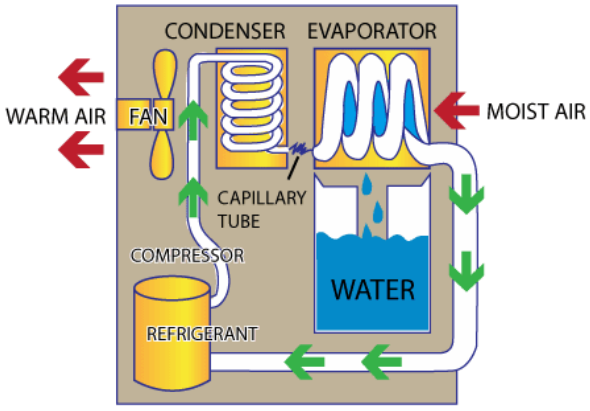

Figure 9. Refrigeration Dehumidification process. (12)

Absorption/adsorption dehumidifiers rely on a mechanical means of extracting water, usually employing a rotating disk with extremely high surface area coated with

silica to attract and hold the water in one process, while in a regeneration process, hot air absorbs water from the other side of the disk and releases it on the surface of the condenser.

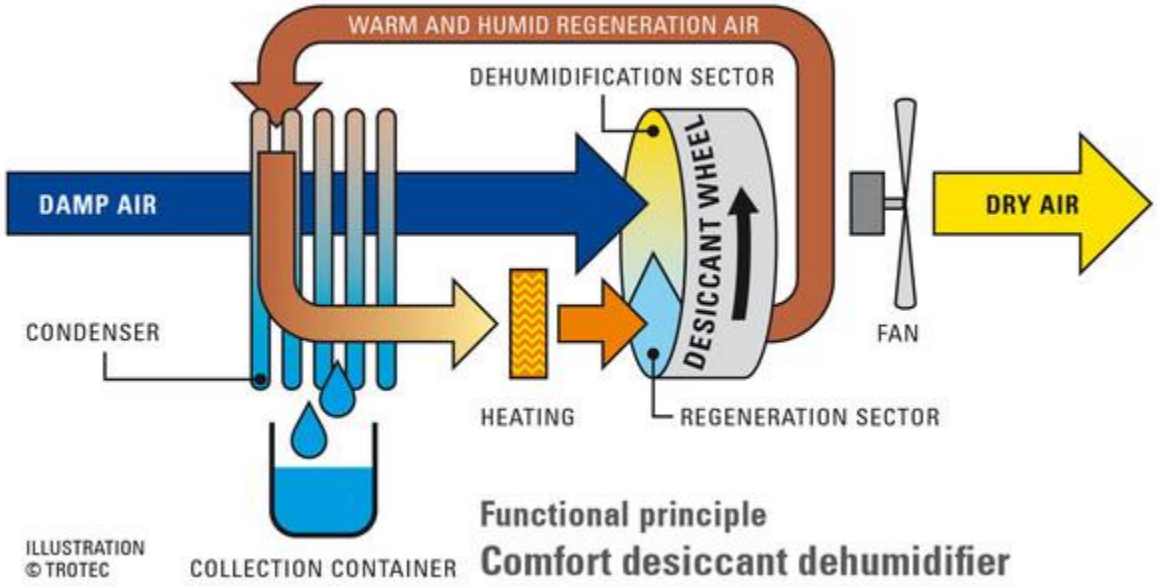

Figure 10. Absorption/adsorption dehumidification process. (13)

2.2.5 Thermoelectric Cooling Products

There are small TEC (thermoelectric cooling), or Peltier element, powered dehumidifiers on the market now, and while not as efficient as vapor compression based models, they are very compact and less noisy. These dehumidifiers tend to be used for smaller scale applications, such as bathrooms, as they do not have the same capacity as the larger vapor compression models. An example device, the Eva-dry 2200, is shown below in Figure 11 below. The manufacturer claims that the device will collect

about 20.5 ounces of water per day at 72 W power consumption, dependent on relative humidity. (14)

Figure 11. Eva-dry 2200 Peltier element dehumidifier. (14)

2.2.6 Peltier Elements

Peltier elements use electric energy to create a heat flux across a metal plate. They operate by running current through two semiconductors, one n-type, one p-type, sandwiched together and connected in thermal parallel and in electrical series. This is shown in Figure 12. It uses the same principle as a thermocouple, where a current is formed by two different metals reacting differently to a temperature gradient, but in reverse. This is based on the fact that charge carriers diffuse from the hot side to the cold side of a material under a temperature gradient. In this case, the charge carriers of an n-doped semiconductor are electrons, and the charge carriers of a p-doped semiconductor are “holes.” By connecting the two materials in a circuit, the movement

of these electrons and holes can be harnessed to create a current. The Peltier element uses this same principle, but in reverse; current is supplied to move the charge carriers, which then moves heat from one side of the element to the other. A simple model of this is shown in Figures 12 and 13.

Peltier elements are a less efficient method of cooling than vapor-compression (about ¼ as efficient) (15), but they do have some distinct advantages. They have no moving parts or fluids, so shape and size are very flexible. Leaking is also not an issue. They have long lifespans, and are easily controllable by changes in electrical input. They tend to operate more efficiently at lower temperature differences, as they have to dissipate the heat from the hot side as well as the heat generated by the electrical power input. (16)

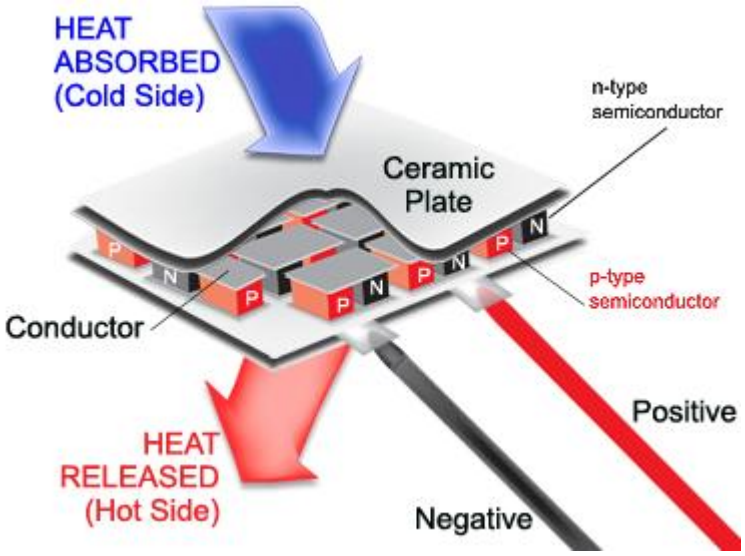

Figure 12. Peltier element basic interior (17)

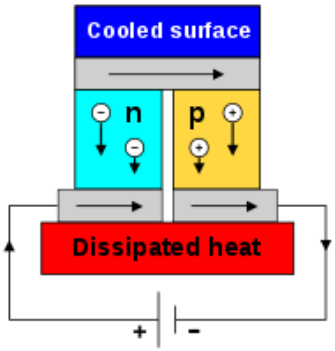

Figure 13. Simple model of the Peltier effect. (18)

In Peltier elements there is a linear relationship between cooling capacity and temperature difference, as shown below in Figure 14. The graph shows that the maximum cooling capacity occurs at the lowest temperature difference.

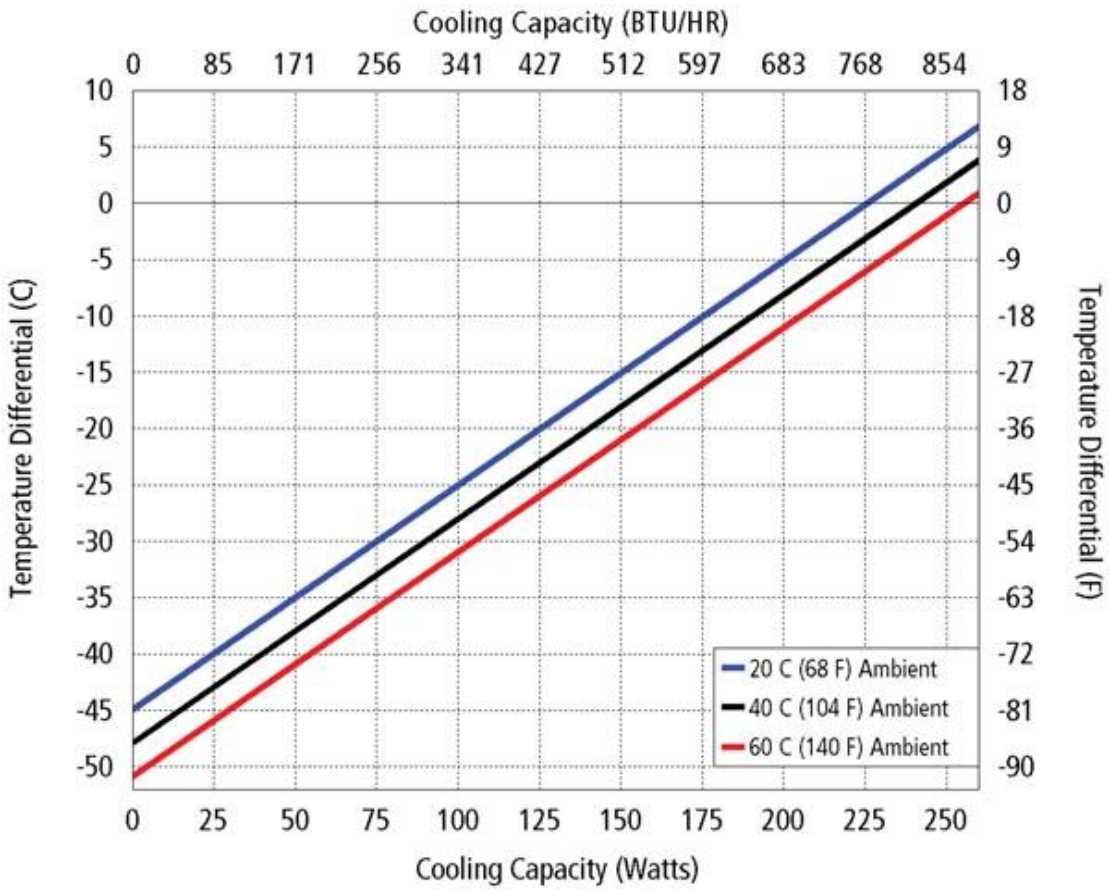

Figure 14. Cooling capacity as a linear function of temperature difference across the sides of a selected Peltier element. (19)

2.3 Background Science

2.3.1 Weather and Fog Information

There are two major types of fog in California, radiation fog and advection fog. For both types, fog is formed when the relative humidity of the air reaches 100%, and water vapor condenses on tiny particles in the air, creating the “foggy” appearance. The fog stays suspended in the air due to an extremely low terminal velocity, and slight convection currents keeping the particles afloat. Radiation fog is produced by rapid surface cooling due to radiation heat loss. It usually forms at night under clear

skies with calm winds when heat absorbed by the ground during the day is radiated into space. As the ground continues to cool, the moist air reaches saturation and fog forms. Radiation fog is always found at ground level and usually remains stationary. According to the National Weather Service Weather Forecast Office, the depth of the radiation fog can vary from 3 feet to about 1000 feet. (21) Radiation fog commonly forms on floors of interior valleys.

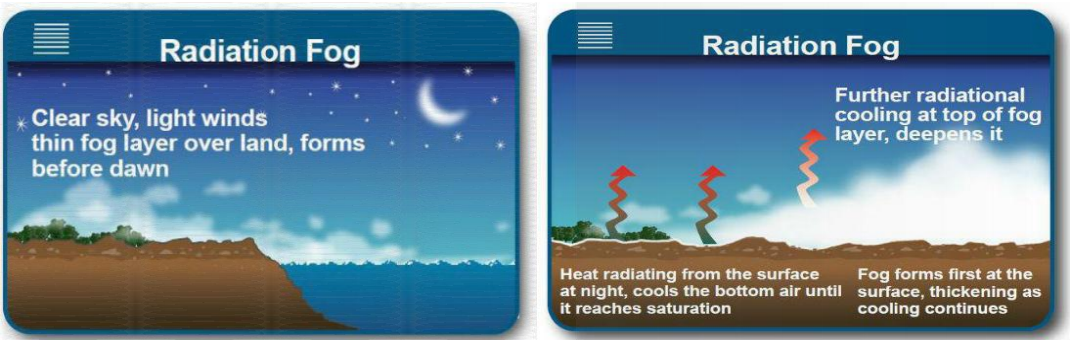

Figure 15. Radiation fog formation. (22)

The other type of fog in California is advection fog. With advection fog, the condensation is caused by the horizontal movement of warm moist air over a cold surface.

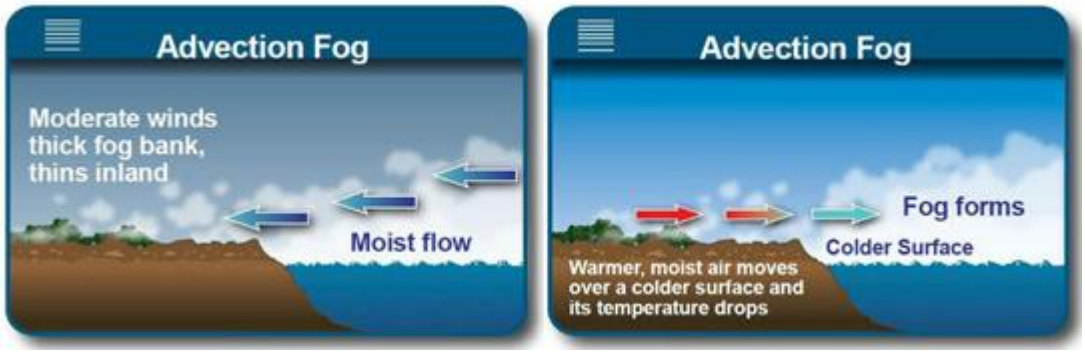

Figure 16. Advection fog formation. (22)

Advection fog is common along the California coast in summer. When warm, moist air from the ocean flows over a cold inland area, the moist air will be cooled from below. If the air is near saturation, moisture will condense out of the cooled air and form fog. In both cases the air above the surface is cooled to its dew point (100% relative humidity).

A clear sky, light winds, relatively high humidity and a stable atmosphere are needed for the formation for both radiation fog and advection fog. (23) A clear sky allows the long wave radiation to leave the earth's atmosphere, instead of being trapped between the ground and the clouds. With a light wind, fog will form at ground level. If the wind is too strong, the condensation will instead form low stratus clouds.

2.3.2 Condensation Types

There are two types of condensation: dropwise and filmwise condensation. Dropwise condensation is where the vapor condenses on a surface that is not already wetted by the condensate, while filmwise condensation is where the vapor is condensing on thin layers of condensate already present. The heat transfer coefficient of dropwise condensation is often 10 to 20 times higher than filmwise condensation. (24)

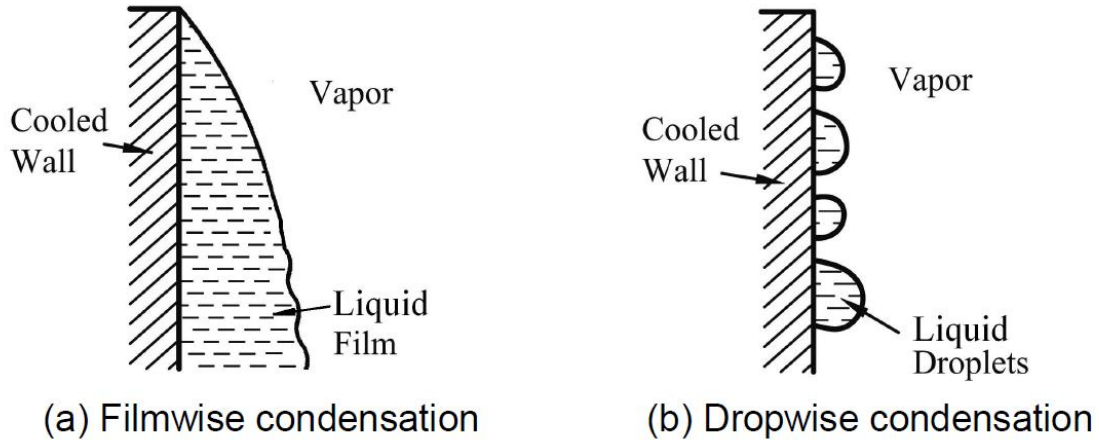

Figure 17. Filmwise and dropwise condensation diagram. (25)

Dropwise condensation requires that the surface be continually exposed to the vapor by the formation and coalescence of drops, and the wiping action of running drops. Drops are formed at nucleation sites on the surface, and they grow until neighboring drops combine. This continues until the drops reach maximum size, and are caused to “drop” due to gravity. (24)

2.3.3 Surface Effects on Condensation

In order to make dropwise condensation possible, a non-wetting agent is usually required. One such agent is polytetrafluoroethylene, or Teflon. The goal of these “dropwise promoters” is to make sure that the vapor condenses in drops rather than in a film. One of the more cutting edge ways that this can be accomplished is by having a complex pattern of hydrophilic and hydrophobic materials. (24)

A more common and affordable dropwise promoter, such as Teflon, is ideal for a project of this scope. Teflon coatings have been found to be effective in promoting

dropwise condensation for use with steam cycles. Teflon is best bonded to metals, and aluminum in particular. This is because the Teflon can fill in the holes in the porous oxide layer of the aluminum, providing a strong mechanical bond. It is important that the Teflon layer be kept thin (ideally in the ten-thousandths of a centimeter range), because the thermal conductivity of Teflon is low, so a thick layer will impede surface cooling. (26)

2.3.4 Pressure Effects on Condensation

Increased pressure increases the dew point of vapors, as shown in Figure 19 below.

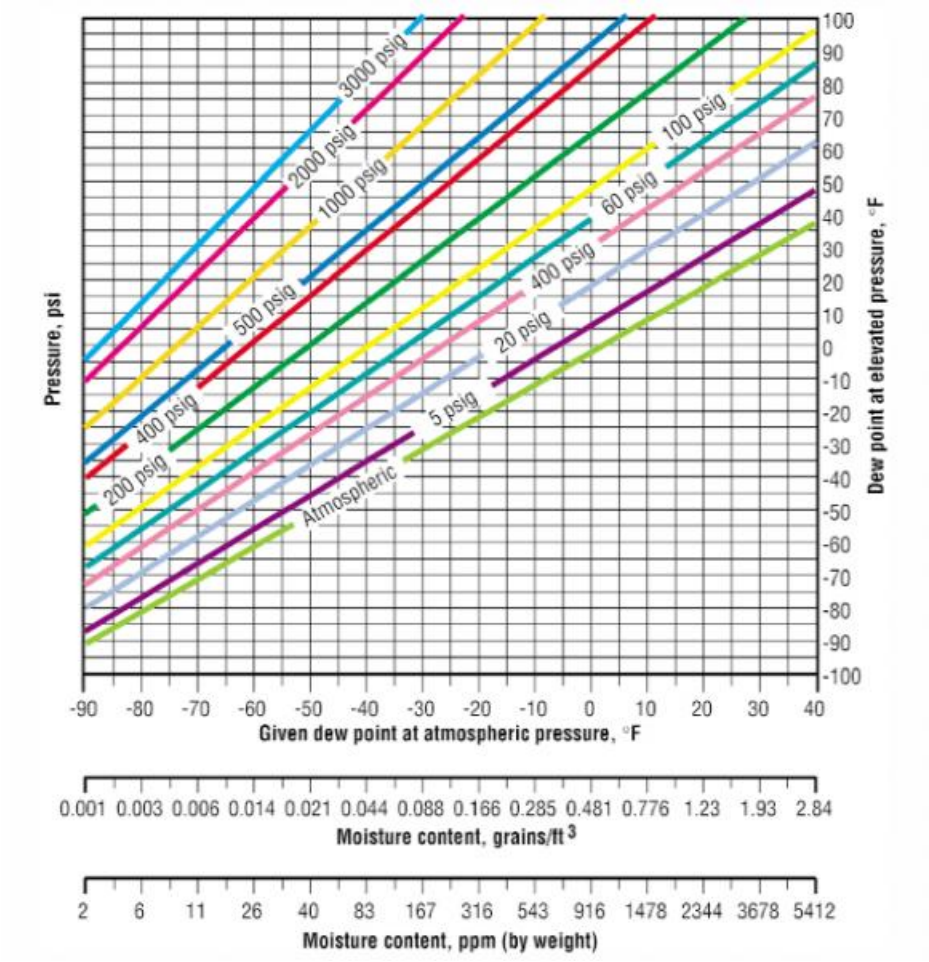

Figure 18. New dew point vs. old dew point based on pressure difference. (27)

Using pressure to modify the dewpoint can be very useful when working with pure vapors, but it is not as useful for condensing water. This is because pressurization takes a large amount of energy, and when working with an air and water vapor mixture, a lot of the energy used to pressurize the mixture is being used to pressurize the air,

which is useless for this application. As such, pressurization techniques are not generally useful for atmospheric water harvesting at the moment.

2.4 Initial Vapor Compression Prototype

The initial design, shown in Figure 19, consists of a refrigeration cycle where the evaporator sits in a fan-fed rectangular duct. The refrigeration cycle is powered by a 2490 btu/hr (730 W) rated Copeland condensing unit, which is composed of a ¼ hp (186 W) semi-hermetic compressor, a fan-blown condenser, and a receiver. This unit is connected via $1/8^{th}$ inch (3.175 mm) copper tubing to four evaporators within the duct. The copper tubing is routed with the help of ¼ inch (6.35 mm) brass compression fittings (unions and tees). The duct is rectangular and made of ¼ inch (6.35 mm) polycarbonate plastic.

The evaporators are positioned such that there is a pair of front and back evaporators side by side with another identical pair. The evaporator pairs are connected in series, with the coolant running through the back evaporator first and the front evaporator second. The moist air is drawn into the duct using a pair of fans (one per pair of evaporators). These fans are connected to power throttlers and can be run using a variety of flowrates to test the optimal operating condition for condensation, but are rated for 0.11 m^3/s. The four evaporators and two fans are connected to the inside of the duct using bolts fixed to the duct floor. The coolant (R134a) lines run out of the top portion of the back of the duct and connect the evaporators to the condensing unit. Since one pair of evaporators is connected in parallel to the other pair, the entering and

exiting lines meet in a T-joint before and after the condensing unit.

In order to control the coolant flowrate, two expansion valves and a ball valve are connected in parallel between the receiver and the evaporators. The ball valve controls broad flowrate change, while the expansion valves are used to fine-tune the system flowrate. Two temperature and pressure gauges are used to monitor the high-side and low-side pressures and temperatures of the system. The entire duct is screwed to a fixed wooden board along with the condensing unit. The condensing unit is directly behind the duct in order to route some of the cold air coming out of the duct through the condenser. The duct is mounted at a 3 degree angle, tipped forward as seen in Figure 20. This allows condensate to flow out the front of the duct, which has a small lip with a break in one corner to channel the condensate into a collection bin. This requires that the system be mounted on an elevated surface. The entire system is mounted on a table with wheels to allow for some mobility. The power cords from the two fans and the condensing unit are connected through a power strip, a wattmeter, and then plugged into a standard wall outlet. A system diagram is shown in Figure 21.

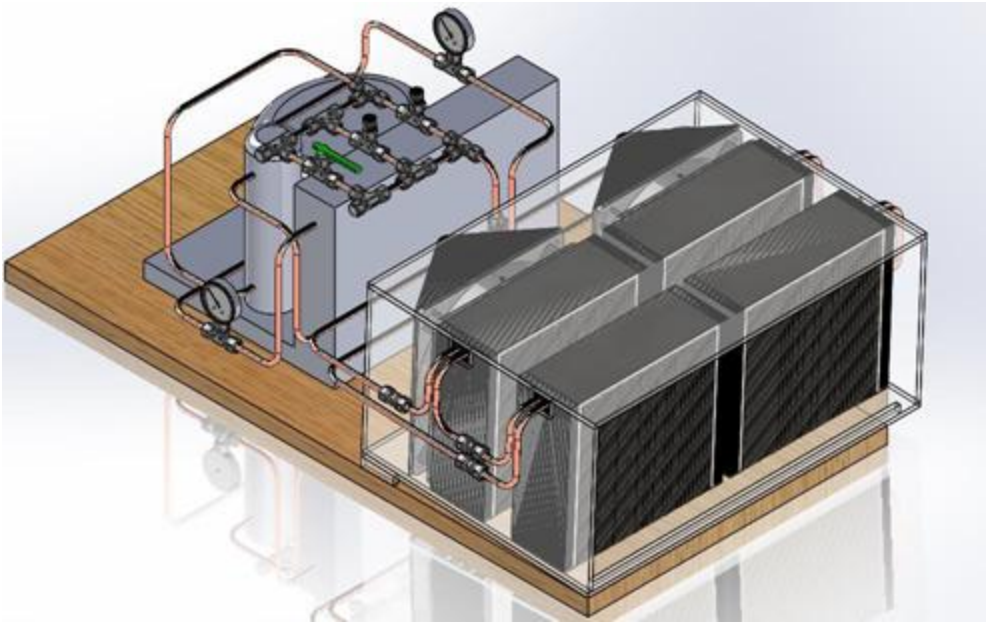

Figure 19. Isometric view of the initial prototype design.

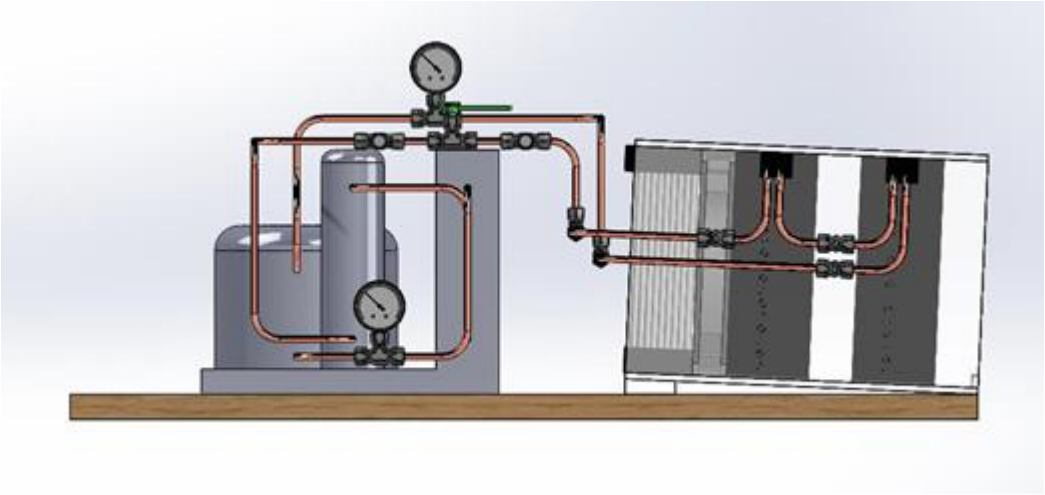

Figure 20. Side view of the initial prototype design.

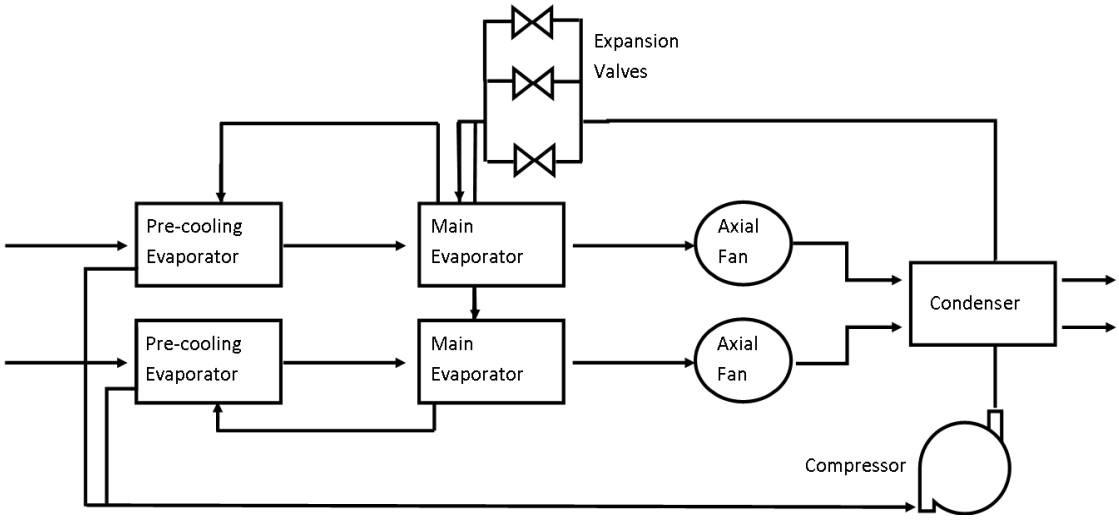

Figure 21. Initial prototype design system diagram.

Chapter 3: Design Development

3.1 Vapor Compression Prototype Modifications

The vapor compression prototype was modified for this project as follows. Two ball valves were added to one evaporator set branch, to allow this branch to be bypassed. This puts the prototype into the “single evaporator” (two evaporators in series, one set of evaporators) mode, which concentrates the cooling power into the remaining evaporator set, resulting in higher refrigerant flowrate through the evaporators, and more cooling in the forward evaporator. Additionally, cutting off the other branch can also slightly change the refrigerant charge in the system based on whether the system has been running when the valves are closed. If it has been running, some portion of the volume of refrigerant within the sealed branch will be vapor, and more will be left in the system. However, the mass of refrigerant actively used during operation is largely controlled by the receiver.

The refrigeration charge was lowered from 12 to 11 oz in order to better accommodate the single evaporator configuration. The table legs are now adjustable to allow for a steeper tilt on the duct to promote more regular drainage. The prototype is shown below in Figure 22.

Figure 22. Vapor compression prototype picture.

3.2 Thermo Electric Cooling Prototype Design

The magnitude of the heat flow and the high temperatures produced on the “hot side” of the Peltier element requires that there be a heat sink attached to that side which is cooled in some way, the simplest methods being either by fan, or by water cooling. The condensation surface must be connected to the “cold side” of the element in order to condense any water. Because of this, the logical design was to sandwich the element between the heatsink and the condensation surface, with some thermal paste in between to ensure good thermal conductivity in the contact areas. Bolts were used to secure the sandwich. Attaching the heatsink to the condensing surface via four bolts

allows for easy swapping in-and-out of the multiple condensing surfaces. All setups use a polycarbonate divider that sits between the heatsink and the condensing surface in order to prevent the hot air blowing out of the heatsink from warming up the back of the condensing surface.

The heatsink chosen for this design is a fairly standard cpu heatsink and fan combination, the Arctic Alpine 11 Plus. This model uses a pulse-width modulated fan that is wired to run on maximum speed at all times. The Peltier element is a TEC1-12706 from Eathtek, which is rated at 12V 5.8A. The thermal paste is Arctic Silver 5, which is a 99.9% pure micronized silver paste designed to fill any gaps in the contact area between components and provide a highly conductive bridge between them. The Peltier element, heatsink, and fan configuration are shown in Figure 23. The full prototype with the passive heatsink condensing surface attachment is shown in Figure 24.

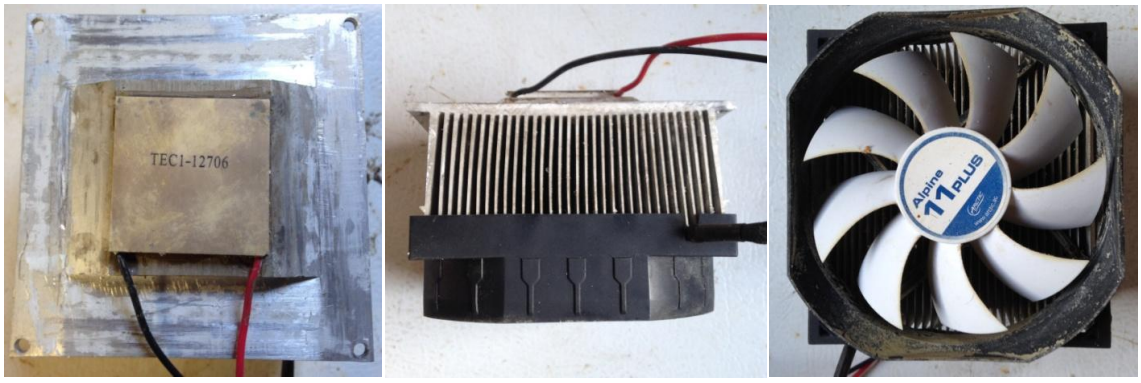

Figure 23. Peltier element, heatsink, and fan configuration.

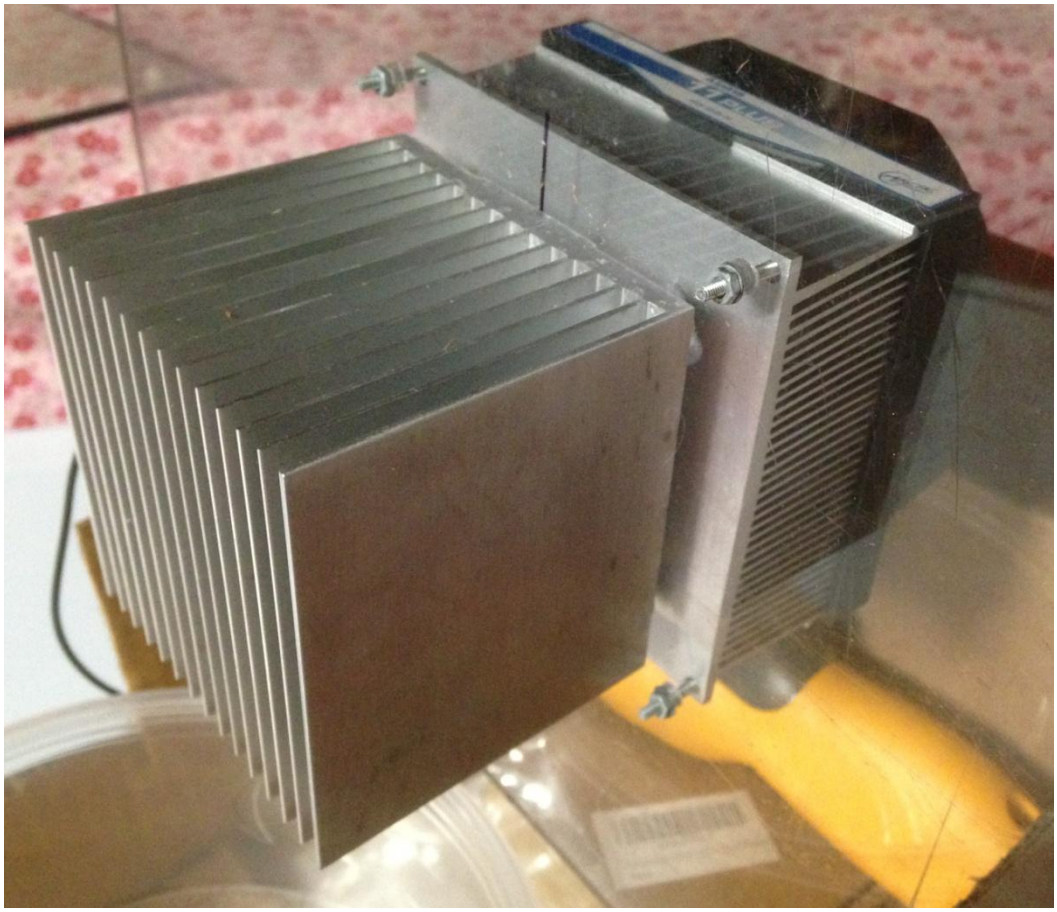

Figure 24. TEC prototype with passive heatsink condensation surface attachment.

The Peltier element is connected to a 13.8V, 10A DC power supply, and draws about 3A when air-cooled. The heatsink fan is wired in parallel with the element, and draws about 0.36A. The power supply is shown below in Figure 25.

Figure 25. Pyramid regulated 13.8V, 10A DC power supply.

The modularity of this design allows for testing of many different condensing surfaces described below.

3.2.1 Aluminum Plate

An aluminum plate, approximately 10” by 5”, with a thickness of ⅛” has been chosen. The thickness of this plate and the higher thermal conductivity of aluminum allow this collector to spread the cold area fairly evenly across the plate. The aluminum plate attachment is shown below in Figure 26.

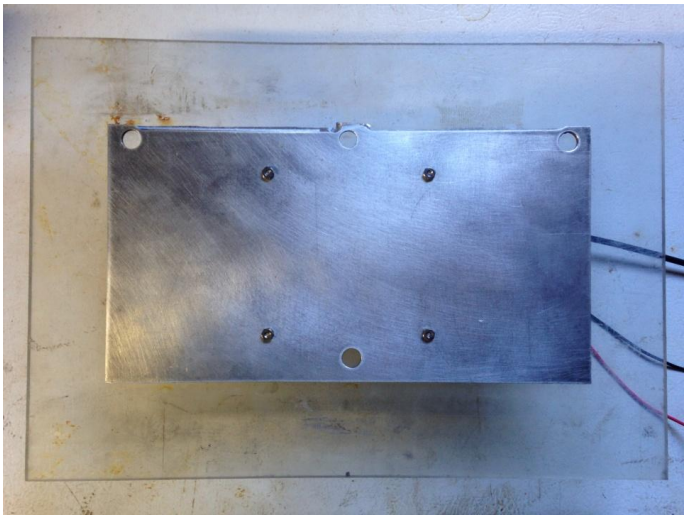

Figure 26. Aluminum plate collection surface attachment on the TEC prototype.

3.2.2 Teflon Pan

The Teflon pan is from a Farberware Cookware Aluminum Nonstick 11-Inch Square Griddle, cut to approximately 10” by 5”. The Teflon non-stick coating promotes smaller beads of condensation to form on the surface, and for a much “drier” surface when the water is wiped from it. The Teflon pan attachment is shown in Figure 27.

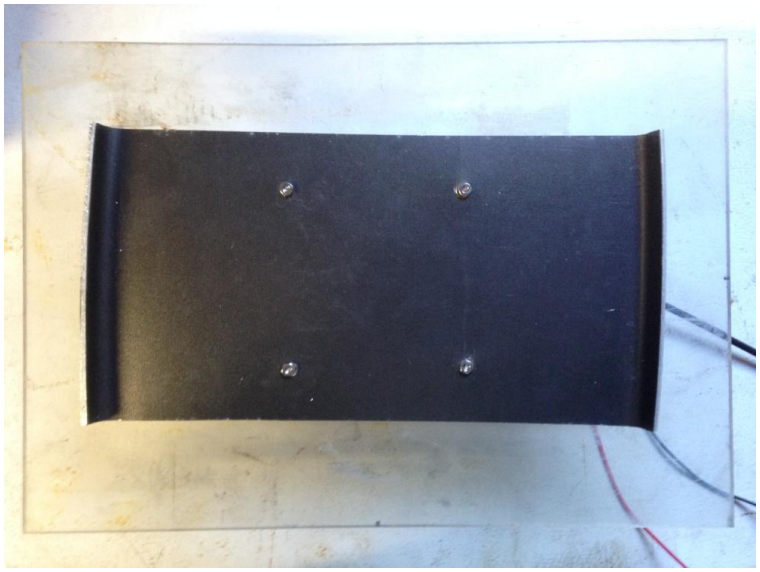

Figure 27. Teflon pan collection surface attachment on the TEC prototype.

3.2.3 Fanned Plate

Two aluminum plates are stacked together and fan out from the center of the aluminum base plate. This provides more surface area than a regular plate, but less airflow restriction than the heatsink. The fanned plate attachment is shown below in Figure 28.

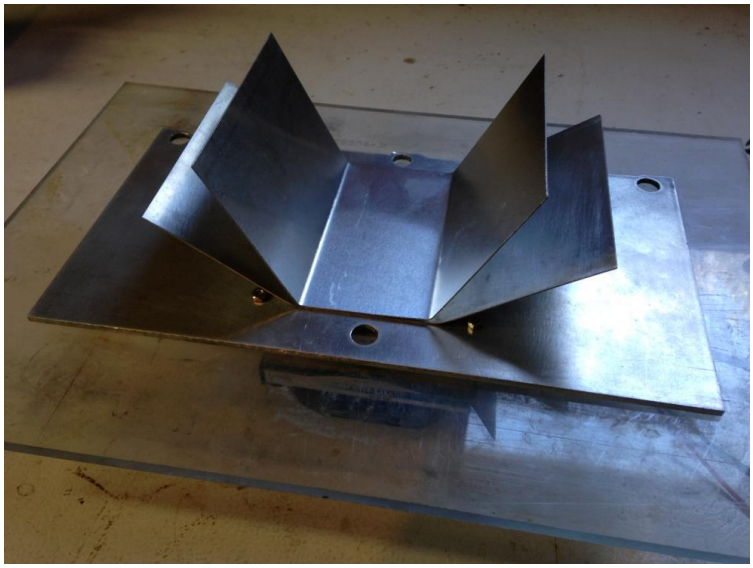

Figure 28. Fanned plate collection surface attachment on the TEC prototype.

3.2.4 Passive Heatsink

An Arctic Alpine M1, meant for cooling CPUs, has been selected as a passive heatsink. It has relatively wide fin spacing for efficient natural convection and the largest surface area of any of the condensing surfaces. The heatsink attachment is shown above in Figure 24.

Chapter 4: Experimentation

4.1 Experimental Goals

The purpose of the experiments is to determine how much water can be collected per amount of energy consumed, and how different environmental conditions and device configurations affect this collection rate.

4.2 Vapor Compression Prototype Testing

The vapor compression prototype is placed in the humid environment outside. The power strip is plugged into a standard 120V AC socket, with a wattmeter between the power strip and wall. All valves are opened (to maximum in the case of the expansion valves) and the evaporator fans are turned on from the power strip. Fans are set at the desired speed. If desired, the regeneration hood is assembled over the duct. After all this is in place, the wattmeter is set to start counting the energy usage in kilowatt hours, and the compressor is turned on from the power strip. After a brief warm up period (approximately 5 minutes) the cut-off valve is closed for a single evaporator set experiment, or left open for a double evaporator experiment. The expansion valves are then closed to dial in the vaporization pressure and temperature in the evaporators. Water drips from the spigot and is collected in a graduated cylinder, where the collected amount of water is measured against the consumed power at several points during the test. Temperature and relative humidity are also recorded at this time. Once the test is completed, the components are returned to their starting states in reverse order.

Many of the environmental variables of experimentation are determined by the weather (temperature, humidity, wind, fog). As a result, tests are performed in a variety of temperature and humidity conditions.

Tests are performed on Cal Poly campus, in San Luis Obispo, Atascadero, Morro Bay, and Santa Margarita at all times during the night and early morning during the maximum relative humidity condition. Flowrate is varied for the tests in order to generate the curves seen below. Data is taken at a fairly constant vapor-compression cycle operation point, with a high-side pressure of 620 kPa, and a low-side pressure of 138 kPa, with a saturation temperature of 25°F. This operation point is noted by the formation of frost on the first 2-3 coils in the back evaporators. The data for this experiment represented in Figure 29 below can be found in Appendix A, Table 1A.

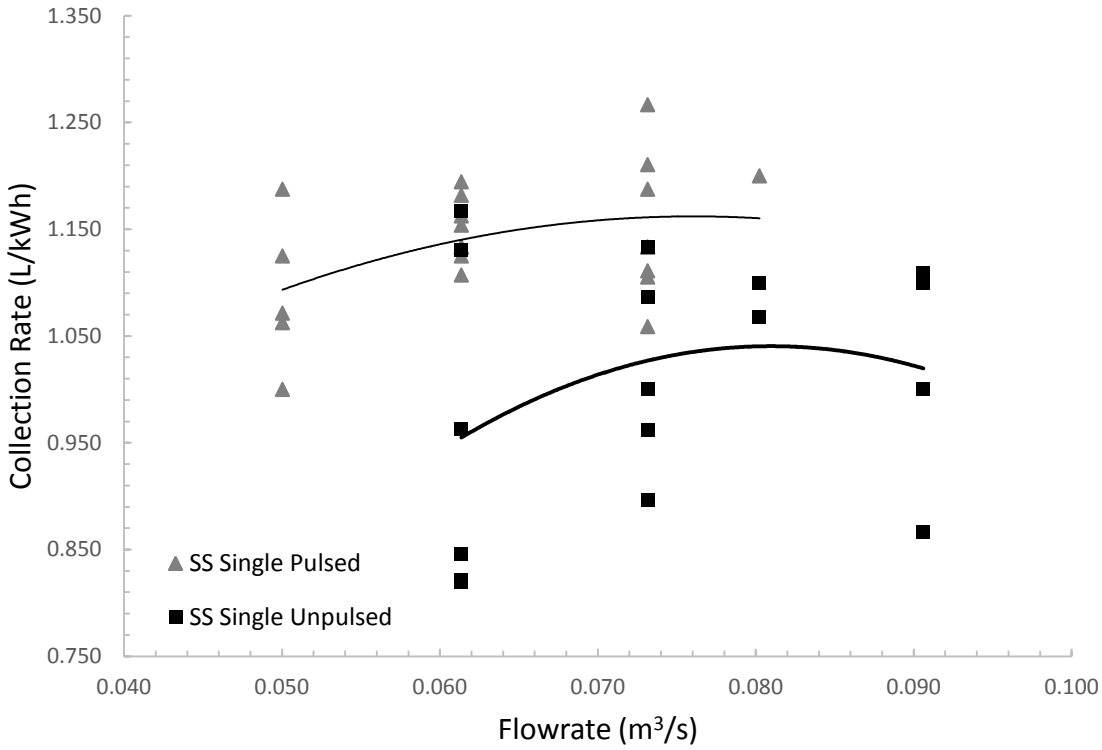

Figure 29. Vapor compression prototype collection rate as a function of flowrate.

Figure 29 shows the steady state results for high humidity (85-100%) tests performed in the single side evaporator configuration, with pulsed and unpulsed tests. “Pulsed” denotes an operating condition where the fans were turned up to maximum speed for 10 seconds every twenty minutes in order to free up condensation surface area by dislodging condensate droplets from the evaporator. The steady state rate is the amount of water collected divided by the power used from the first drop collected to the end of the test period. The steady state collection rate is meant to give an idea of how the prototype would perform during long periods

of operation. As a reference, the startup throughout all of the tests averaged about 0.17 kWh of energy usage, and lasted 25-30 minutes.

Trendlines are added in order to show the approximate relationship between flowrate and collection rate. There is a slight curve in the collection rate lines, suggesting that there may be a flowrate that results in the maximum collection rate. This maximum occurs at 0.081 m^3/s for the unpulsed trials and 0.073 m^3/s for the pulsed trials. It is suspected that this maximum is due to the flowrate providing an optimal balance between providing maximum water vapor movement through the system while still allowing enough time for the air to be cooled to the dew point and the water to be condensed. Too low a flowrate results in less water moving through the evaporators than they can condense, wasting cooling energy, while too high a flowrate results in wasting cooling energy to cool air that moves too quickly through the evaporators to reach the dewpoint. In thick fog conditions, it is expected that this maximum would shift to the right (higher flowrate), as there would be no need to allow for more time to cool the air to the dewpoint, as it is already at the dewpoint, and laden with liquid water.

The graph also shows that pulsing yields a higher water collection rate. It is observed that after a pulse, a small surge of water leaves the evaporators. Increasing the flowrate causes many of the condensed water droplets on the evaporator fins to start rolling and collecting other droplets before falling off of the fins. This frees up that space for more condensation to occur, as condensation is easier on a bare surface than on other droplets. The increase in collection rate achieved in pulsed trials

compared to unpulsed trials drops slightly at higher flowrates. Higher flowrates promote more droplet movement, making a pulse less effective relative to lower flowrate trials.

4.3 TEC Prototype Testing

4.3.1 Surfaces Comparison

The TEC prototype collection surface is placed vertically facing a Pureguardian H4500 ultrasonic humidifier. The TEC and cooling fan is connected to a DC power source, and powered at 12V 6A. The power source is then plugged into a wattmeter, and into wall socket. The humidifier is set so that the humidity dial is pointing straight right. This setting provides enough moist air to simulate foggy conditions without condensation occurring on nearby non-cooled surfaces. This condition is intended to ensure that the test surfaces themselves have as strong an impact as possible on the experiment results. The humidifier jet of humid air is pointed so that it directly hits the center of the collection surface, pluming outward as shown in Figure 30. Water drains into a plastic funnel, and into a collection container. At the end of the test, temperature and humidity measurements are taken, and the water in the collection container is transferred to a graduated cylinder and measured. The water collected is then measured against the consumed power. For this experiment, the surfaces being tested are an aluminum plate, a Teflon coated pan, a fanned aluminum plate, and an aluminum heatsink. The aluminum plate and Teflon pan have test trials where the surface is wiped clear with a rubber wiper every hour, denoted as “cleared” hereafter. Tests where the

surface is left untouched are “uncleared.” Table 2 and Figure 31 show the average collection rate of the tested surfaces. Table 2, and following tables, also include the collection rate in kWh/m^3, a common unit for water collection, though this unit is not represented in the associated figures. Figure 32 shows the surface area of the surfaces.

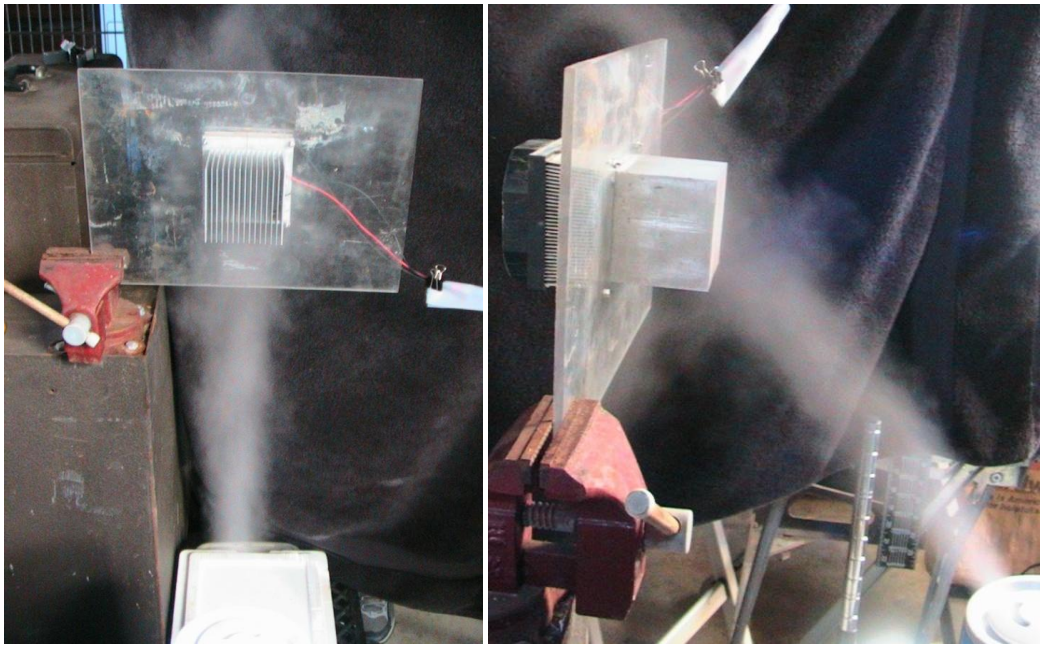

Figure 30. TEC prototype experiment humidifier flow example with heatsink collection surface.

Table 2. Average Collection rates for uncleared and cleared trials of TEC Prototype surfaces: aluminum plate, Teflon Pan, fanned plate, and heatsink.

Aluminum Plate	Average L/kWh	Uncertainty (±)	Average kWh/m^3	Uncertainty (±)
Uncleared	0.058	0.009	17130	2594
Cleared	0.067	0.012	15034	2674
Pan				
Uncleared	0.074	0.006	13511	1137
Cleared	0.087	0.009	11524	1212
Fanned Plate				
Uncleared	0.103	0.013	9747	1238
Heatsink				
Uncleared	0.123	0.009	8133	567

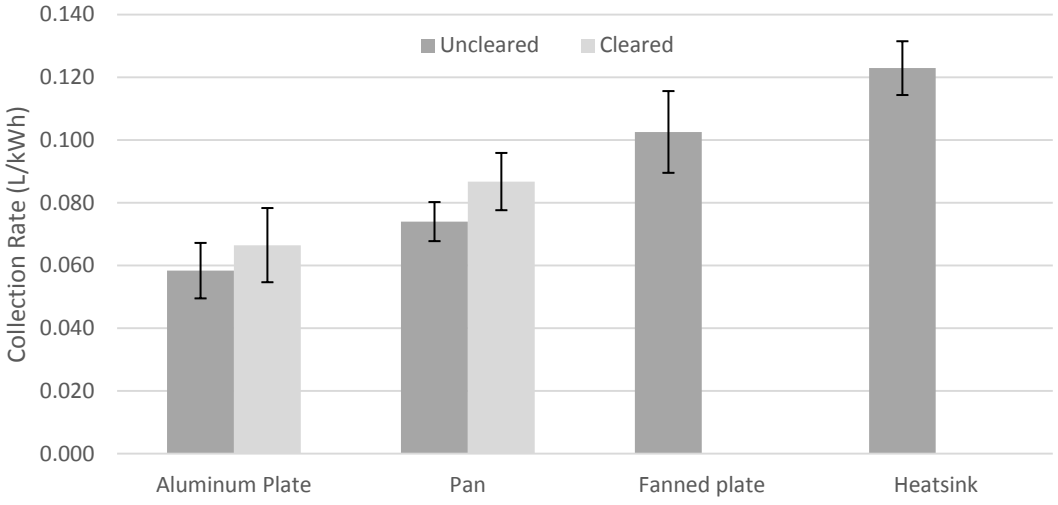

Figure 31. Average Collection rates for uncleared and cleared trials of TEC Prototype surfaces: aluminum plate, Teflon Pan, fanned plate, and heatsink.

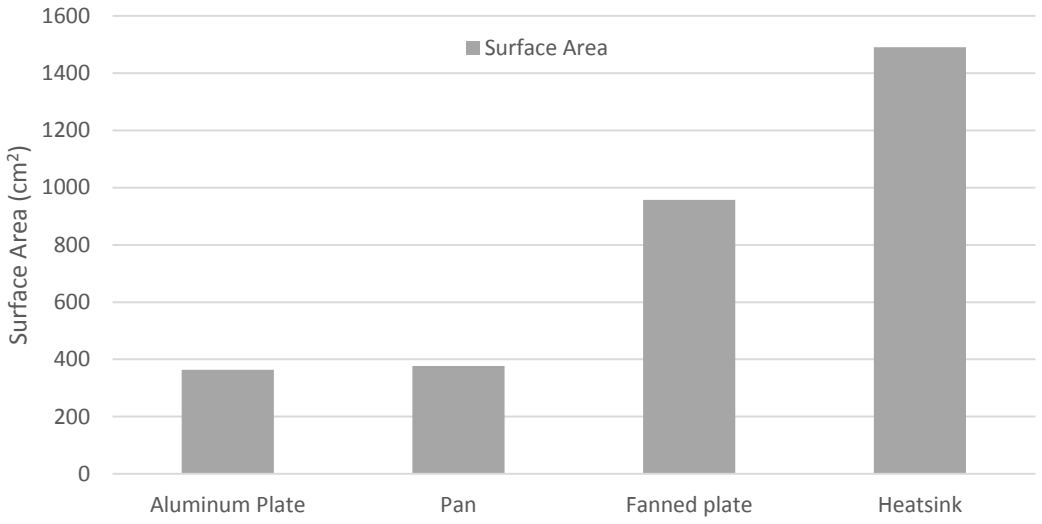

Figure 32. Surface areas of the TEC Prototype surfaces: aluminum plate, Teflon Pan, fanned plate, and heatsink.

Figure 31 shows a steady increase in collection rate across the tested surfaces. The increase from the aluminum plate, to the fanned plate, to the heatsink as the surface area increases is to be expected. However, when compared to Figure 32,

collection rate does not increase at the same rate as the surface area. There is likely a plateau where increased surface area is no longer an effective way to increase collection rate. It makes sense that the TEC element can only efficiently support so large a surface area. This is supported by the observation that in the aluminum plate, pan, and fanned plate experiments, the condensation occurred most strongly around the center of the Peltier element, and slightly waned towards the edges of the collection surface. Given the effectiveness of the heatsink, it seems a compact surface area distribution focused around the cooling side of TEC element is highly efficient. It is also possible that having too large a surface area could be detrimental to water collection rate in less than 100% humidity conditions due to a failure to reach the dew point in parts of the collection surface, though this was not observed in any of the trials of this experiment.

The Teflon pan collects approximately 29% more water than the aluminum plate, despite being roughly the same surface area. This is likely because the Teflon coating causes the condensate to bead up much more than on the aluminum plate, leaving more of the pan's surface area clear for condensation, as well as creating more total surface area (water included) for condensation. A comparison of the surfaces during condensation is shown below in Figure 33. This is doubly important because water condenses more easily on a clear surface than on itself. Clearing also results in an approximately 15% increase in collection rate in both the aluminum plate and Teflon pan trials, as removing the water from the surface frees it up for further condensation. However, the ranges of uncertainty of the cleared and uncleared trials overlap, making the result inconclusive.

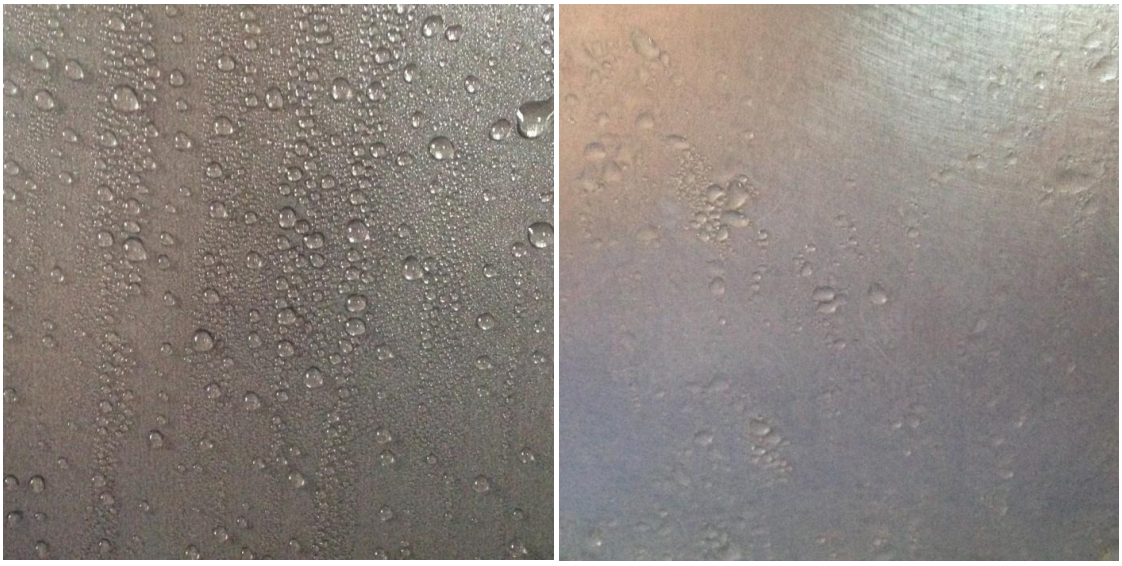

Figure 33. Teflon pan (left) and aluminum plate (right) surface comparison during condensation.

4.3.2 Water Cooling

Water cooling is considered in order to explore the upper bound of TEC prototype performance, and the possible benefits of using condensate regeneratively for heat rejection. For water cooling, the hot side heatsink of the TEC is submerged in a water bath (without the fan) using a sealed plastic sheet divider. A pump is placed in the water bath and directed to shoot a constant jet of cold water at the center of the heatsink. Ice is added to the bath to ensure a constant freezing temperature (0°C, 32°F). A full sized 11 inch Teflon pan is used in this experiment in order to help hold the water bath together. Other parameters are the same as the fan-cooled setup. Figure 34 shows the setup.

Figure 34. Water cooled TEC prototype experimental setup.

Table 3 and Figure 35 show the average water collection rate and temperature difference between the pan surface and the ambient.

Table 3. Average collection rate and temperature difference between the fan cooled and water cooled experiments.

Aluminum Plate	Average L/kWh	Uncertainty (±)	Average kWh/m^3	Uncertainty (±)	Average dT (K)	Uncertainty (±)
Fan Cooled	0.055	0.010	18130	3199	4.7	0.3
Water Cooled	0.109	0.016	9171	1315	8.1	1.0

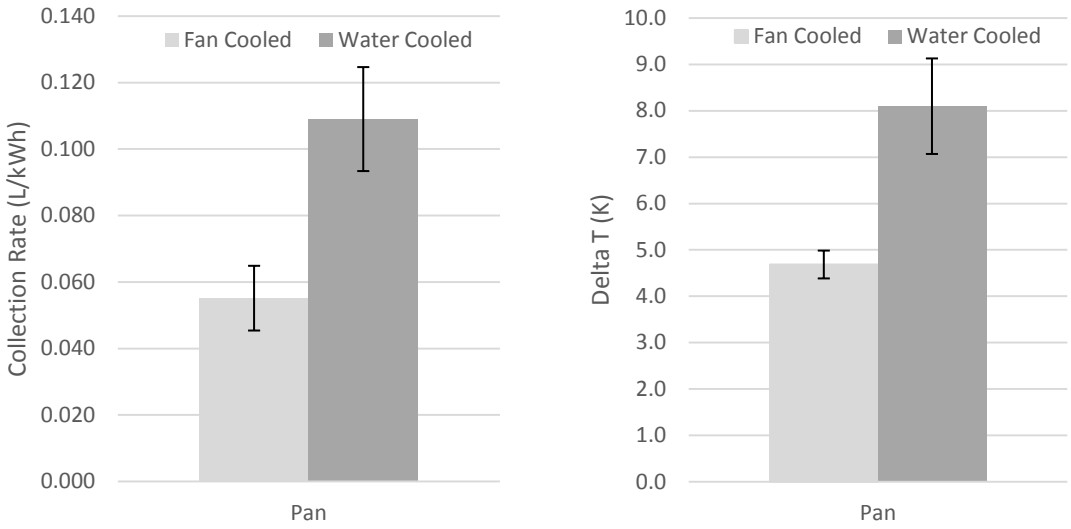

Figure 35. Comparison of collection rates and temperature differences between the collection surface and ambient for fan-cooled and water-cooled Teflon pan setup.

The data above shows a 97.7% increase in collection rate when using water cooling, and an average 3°C drop in cold-side temperature. However, this experiment did not include the power consumption of the water pump, nor the energy required to keep a water source at freezing temperatures. This was done to demonstrate the potential for improvement in the operating conditions of the TEC unit. In fact, if a freezing water source was available, it would probably make more sense to simply run that water through a heat exchanger, rather than use a TEC as an intermediary. That being said, it is clear that the rate of heat rejection on the hot side of the TEC has a very significant effect on its efficiency and the rate of water collection. This experiment helps demonstrate what the TEC prototype might be capable of when operating at near maximum efficiency.

It is also worth noting that the collection rate for the fan cooled test is lower than that of the previous test. This is because the TEC was switched for this experiment,

and this new unit exhibited below average performance. Despite this, it is likely that this same trend would be seen in other TEC units, and it could be used to predict the behavior of those units, subject to further testing.

4.3.3 Tilted Heatsink: Split Flow

The TEC prototype is set up in the same fashion as the normal fan-cooled test, with the humid air directed at the base of the heatsink, but it is tilted about the fan's axis by 0, 15, 30, 45, 60, 75, and 90°, with vertical fins being 0°. This is done by holding the plastic base plate in a vise. Before water collection is measured, the heatsink is cleared of water using a 3/16" hex wrench, scraped between the fins. The purpose of this test is to determine the effect of fin orientation on water collection rate. An example of this set up with the 75° angle is shown below in Figure 36.

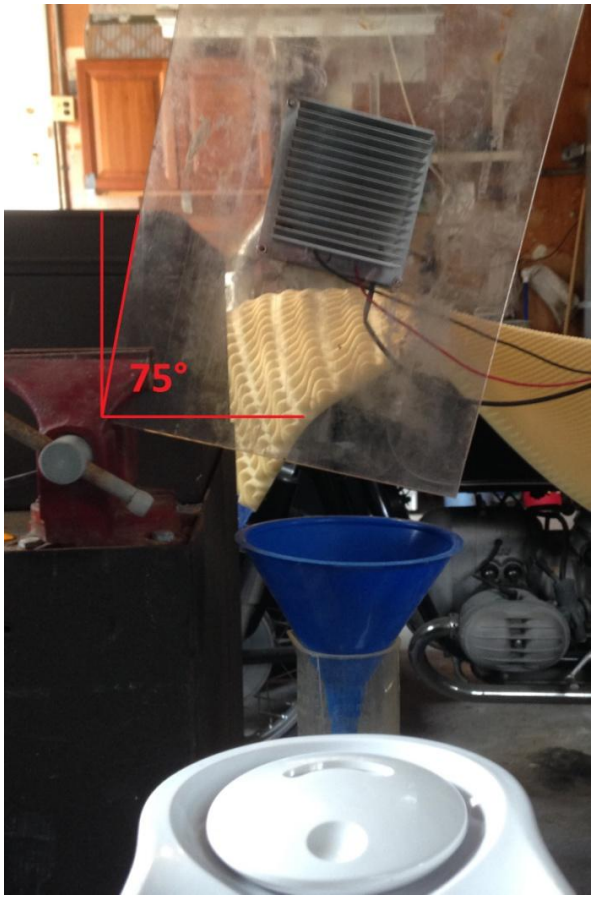

Figure 36. Tilted heatsink experimental setup with 75° tilt.

Table 4 and Figure 37 shows the average collection rates for the different angles tested in the experiment.

Table 4. Average collection rates for the heatsink split flow, tilted at 0°, 15°, 30°, 45°, 60°, 75°, and 90°.

Angle(°)	Average L/kWh	Uncertainty (±)	Average kWh/m^3	Uncertainty (±)
0	0.132	0.018	7577	1026
15	0.157	0.018	6364	724
30	0.177	0.018	5652	571
45	0.213	0.018	4696	394
60	0.249	0.018	4020	289
75	0.234	0.018	4280	327
90 (9 hr)	0.203	0.018	4938	436
90 (24 Hr)	0.127	0.018	7879	1110

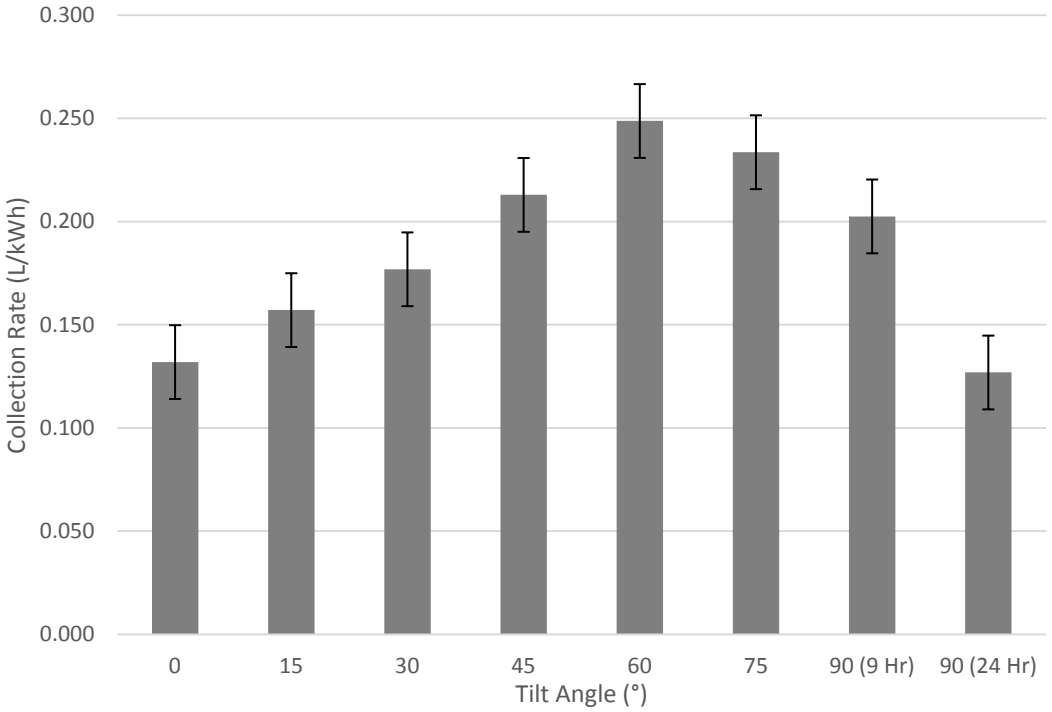

Figure 37. Average collection rates for the heatsink tilted at 0°, 15°, 30°, 45°, 60°, 75°, and 90°.

Figure 37 shows a maximum collection rate occurring at 60°, but it could realistically occur anywhere between 45° and 75°. This is likely due to a combination of condensate bridging and flow profile, which is discussed more thoroughly following the Tilted Heatsink: Through Flow experiment (4.3.4). Starting at 45°, condensate bridging between fins is observed. The amount of water bridging between fins increases as the tilt angle increases. At 90° (horizontal), the entire space between fins eventually fills with water. This is shown in Figures 38-41.

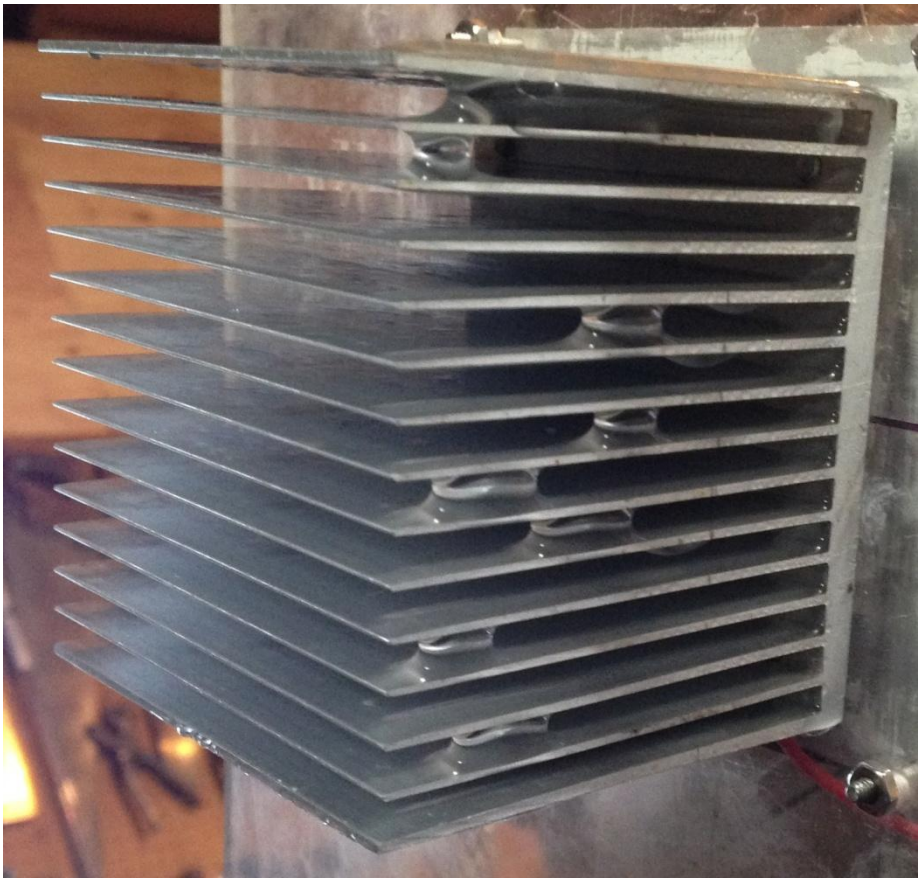

Figure 38. Tilted heatsink split flow condensate bridging at 45°.

Figure 39. Tilted heatsink split flow condensate bridging at 60°.

Figure 40. Tilted heatsink split flow condensate bridging at 75°.

Figure 41. Tilted heatsink split flow condensate bridging at 90°.

Note that Figure 37 has two columns for the 90° tilt angle, one with a 9-hour test duration and one with a 24-hour test duration. The 9-hour test has a much higher collection rate because during the test the heatsink never reached maximum capacity

(when space between fins is completely filled, about 230 ml), and all of the water collected during the test was held by the heatsink for the entire test duration. In other words, nearly all the water collected was collected at the end of the test when the heatsink was drained into the graduated cylinder for measuring. The 24-hour test has a much lower collection rate because the heatsink did reach maximum capacity around the 10-hour mark, where it started collecting at approximately 0.026 L/kWh. Still, the vast majority of the water was collected by draining the heatsink at the end of the test. This shows that the horizontal orientation is highly inefficient over long periods of time, but effective over the short periods, such as overnight, that a device like this would likely be running. More importantly, it suggests that reaching capacity, or too much bridging, is detrimental to collection rate.

4.3.4 Tilted Heatsink: Through Flow

The TEC prototype is set up in the same fashion as the normal fan-cooled test, but it is tilted about the short axis of the base plate by 0, 15, 30, 45, 60, 75, and 90 degrees, with vertical fins being 0 degrees. This is done by holding the plastic base plate in a clamp, which is held by a vise. An example of this set up with the 0° angle is shown below in Figure 42. The purpose of this test is to determine if a different flow regime still produces the same trend shown by the split flow tilted heatsink setup.

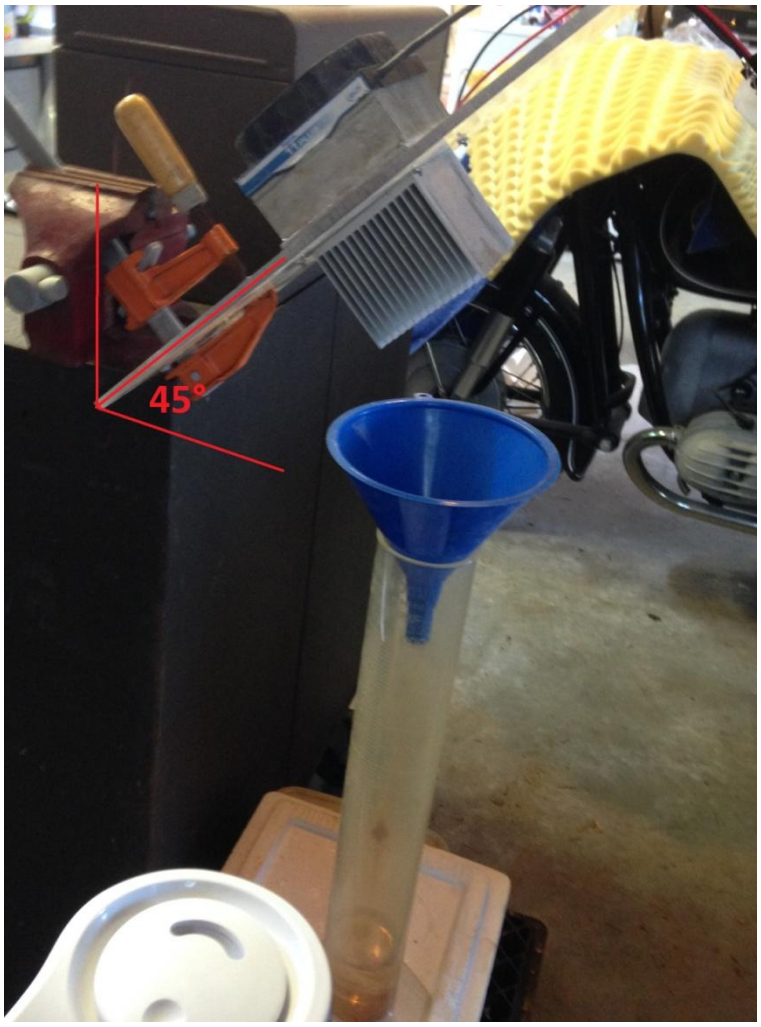

Figure 42. Tilted heatsink through flow experimental setup with 45° tilt.

Table 5 and Figure 43 shows the average collection rates for the different angles tested in the experiment.

Table 5. Average collection rates for the heatsink through flow, tilted at 0°, 15°, 30°, 45°, 60°, 75°, and 90°.

Angle(°)	Average L/kWh	Uncertainty (±)	Average kWh/m^3	Uncertainty (±)
0	0.135	0.018	7429	987
15	0.155	0.018	6471	748
30	0.180	0.018	5561	553
45	0.195	0.018	5122	469
60	0.210	0.018	4755	404
75	0.221	0.018	4519	365
90 (12 Hr)	0.159	0.018	6294	708
90 (24 Hr)	0.130	0.018	7709	1062

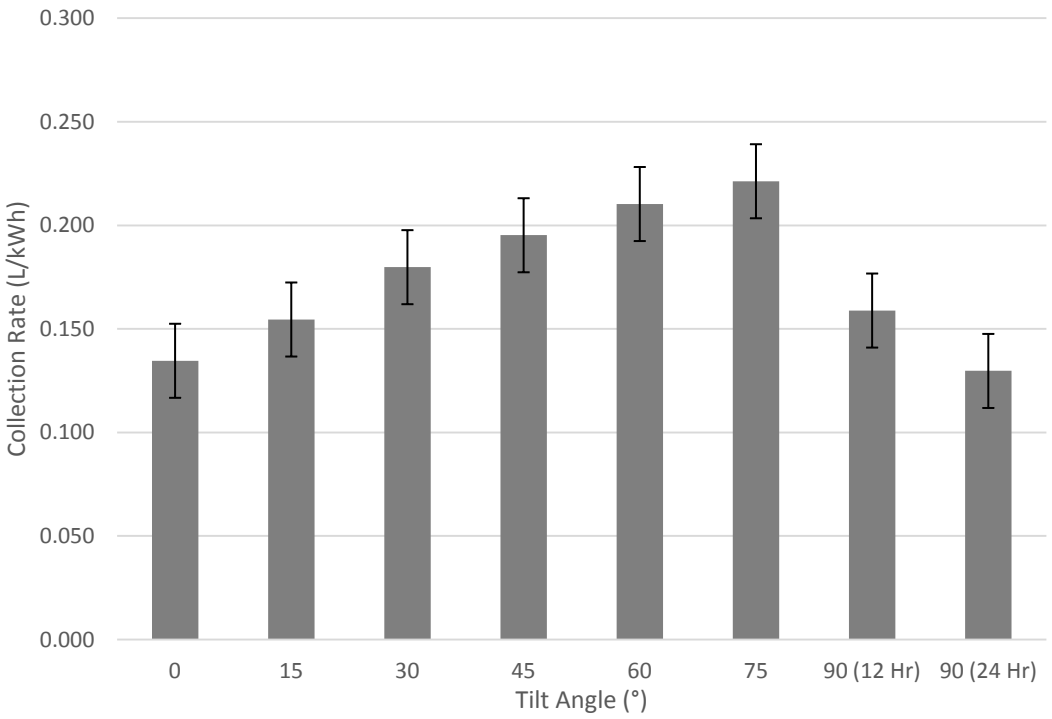

Figure 43. Average collection rates for the heatsink tilted at 0°, 15°, 30°, 45°, 60°, 75°, and 90°.

This flow setup showed a similar trend, but with an overall lower collection rate and less bridging between fins. Condensate bridging between fins now starts at 60°, increasing in severity as the tilt angle increases. At 90° (horizontal), all but a small

passage through the center of the heatsink fills, restricting the airflow through the heatsink, until eventually this fills up as well. This is shown in Figures 44-47.

Figure 44. Tilted heatsink through flow condensate bridging at 60°.

Figure 45. Tilted heatsink through flow condensate bridging at 75°.

Figure 46. Tilted heatsink through flow condensate bridging at 90° (12 Hr).

Figure 47. Tilted heatsink through flow condensate bridging at 90° (24 Hr).

Based on both tilted heatsink tests, it seems that the optimal angle for a heatsink of this geometry is between 60 and 75 degrees. The flow direction has an effect on the overall performance of heatsink, but does not seem to have a significant effect on the trend produced by tilting. The increased performance around the 60°-75° range is possibly due to two effects: the bridging between fins and the weight of the condensate laden air and water vapor.

Slight bridging between fins could be beneficial because it creates more surface area to condense on. This extra surface area (of water) also utilizes the heat transfer that is normally wasted on cooling the condensate before it drains off. The steeper the angle of the fins (from the horizontal), the less bridging can be sustained before the weight of the water overcomes the surface tension, and the water runs off. 60°-75° is possibly the optimal range where the bridging is small enough to create an increase in surface area and minimal flow reduction or blockage. This result is specific to this heatsink geometry, as different fin spacing would change the angle at which this “sweet spot” exists, if it exists at all. Some larger fin spacings would prevent bridging from occurring at all, while smaller ones might bridge even when vertical. Additionally, the flow through the heatsink can also affect bridging. Faster flow can prevent the formation of bridges, as seen in the bridging at 45° in the split flow, but not in the through-flow test, as well as the passage formed in the 90° (12 Hr) through-flow test. However, this effect would not explain the increase seen in the non-bridging cases (15-30°), which is likely due to a more beneficial airflow pattern.

Angling fins toward the horizontal could have a beneficial effect because the density of the oversaturated air makes it sink, relative to the normal ambient air. By angling the fins, it causes this heavier air to slide across the fin surface as it falls out of the heatsink. This might produce a longer contact time between any arbitrary packet of air and the fin surface, or it might create a boundary layer effect conducive to condensation.

4.3.5 Flat Tilted Surface

The TEC prototype is set up with the Teflon pan condensation surface, in similar fashion as the earlier surface experiments. An aluminum duct is now used to channel the moist air from the humidifier to the condensation surface, in order to provide as consistent an angle as possible for the introduction of humid air relative to the pan surface. An aluminum foil funnel is added to the base of the pan to direct all condensate into the collection graduated cylinder. A line of thread runs from the tip of the funnel to a nut submerged in the graduated cylinder, creating a gentle transfer of water with no splashing. The Teflon pan is used in this experiment (as opposed to the aluminum plate) because the way that the condensate drips off of the surface should change with surface orientation, and the Teflon coating should exacerbate this effect, making any observable trends more prominent. The prototype is tilted such that the condensation surface is upward facing at a 15 degree angle from the horizontal, and then rotated down in 15 degree increments for each test until it is downward facing at a 15 degree angle from the horizontal. Several tests are performed at each angle.

Angles closer to the horizontal are omitted for this test due to difficulties managing accurate condensate collection. For the angles 0-15 degrees, it becomes difficult to create the consistent incidence angle of humid air without also introducing condensate drip from the aluminum duct. For the angles 165-180 degrees, the condensate no longer runs down the pan surface consistently, and instead drips from the pan over a wide area. Collecting drips over such a wide area results in an excess of splashing and re-evaporation. An example of the 105 degree setup is shown in Figure 48. The humidifier unit has been changed to a Vicks Ultrasonic Humidifier Model V5100N due to a malfunction in the former unit.

The purpose of this experiment is to determine the effect of surface orientation on a single-side collection surface in isolation. The results can then be compared to the tilted heatsink experiments to determine if the results observed are simply a combination of the effects of an upward and downward facing surface, or if some other effect, such as bridging, has any significant impact.

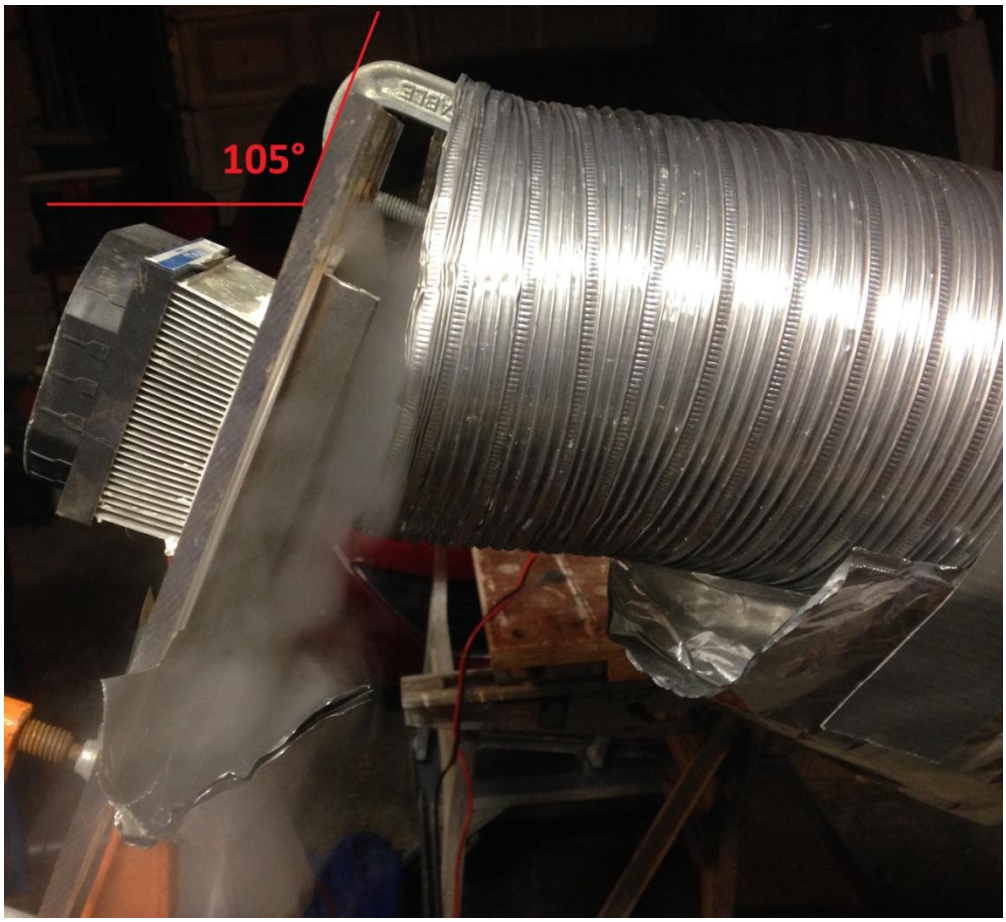

Figure 48. Tilted surface experimental setup with 105° tilt.

Table 6 and Figure 49 show the average collection rates for the different angles tested in this experiment.

Table 6. Average collection rates for the pan surface tilted from 15° to 165° in 15° intervals.

Angle(°)	Average L/kWh	Uncertainty (±)	Average kWh/m^3	Uncertainty (±)
15	0.319	0.012	3134	113
30	0.239	0.012	4192	202
45	0.213	0.012	4704	255
60	0.180	0.012	5562	356
75	0.136	0.012	7339	620
90	0.125	0.012	7972	732
105	0.110	0.012	9110	955
120	0.100	0.012	10024	1157
135	0.100	0.012	9958	1141
150	0.071	0.012	13988	2252
165	0.055	0.012	18217	3820

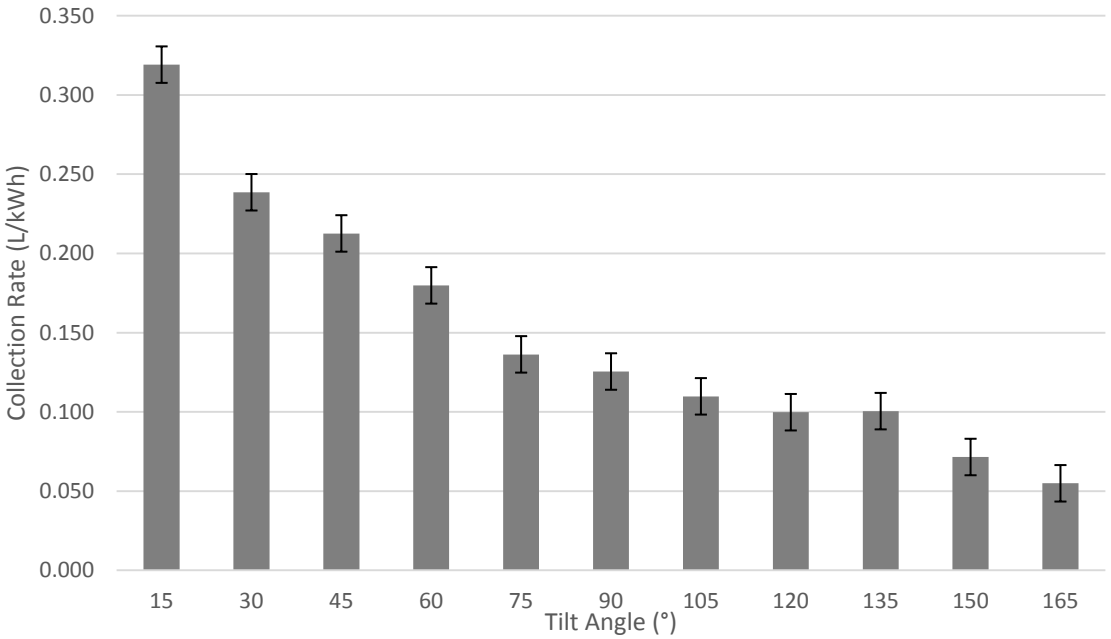

Figure 49. Average collection rates for the pan surface tilted from 15° to 165° in 15° intervals.

Figure 49 shows a maximum collection rate occurring at 15° and steadily declining to a minimum collection rate at 165°. The collection rate at 135° happens to be

a bit higher than 120°, but is within the uncertainty of the measurement. This is likely due to variations in the weather.

This result might be explained by the flow that is created by a cold natural convection surface. While the surface is tilted upward, the cold humid air wants to cling to the surface, providing more time for condensation, while when it is tilted down, the cold humid air wants to fall away from the surface, providing less time for condensation. This same effect could also be caused by the nature of the experimental setup, as the humid air and suspended liquid water mix that is produced by the humidifier is heavier than the surrounding air, and because the prototype is not completely enveloped by the humid air, it creates a flow similar to that of the natural convection. The results are likely an expression of the combination of these effects.

Figure 50 shows the results from the first tilted heatsink experiment, with each angle side by side with the combination of tilted surface angles that would be combined to create that same angle. For example, the 30° tilt on the heatsink (with each fin having two sides) is paired with a combination of the 60° and 120° angles from Figure 49; two single sides representing the upward and downward facing sides of the heatsink fin. Due to the difference in surface area and performance for the two experiments, the collection rates are represented as a percentage difference from the collection rate at vertical position for that experiment. For the tilted surface experiment, the two angles' percent differences are individually calculated, and averaged to find an estimated combined effect to compare to the double-sided fin of the heatsink.

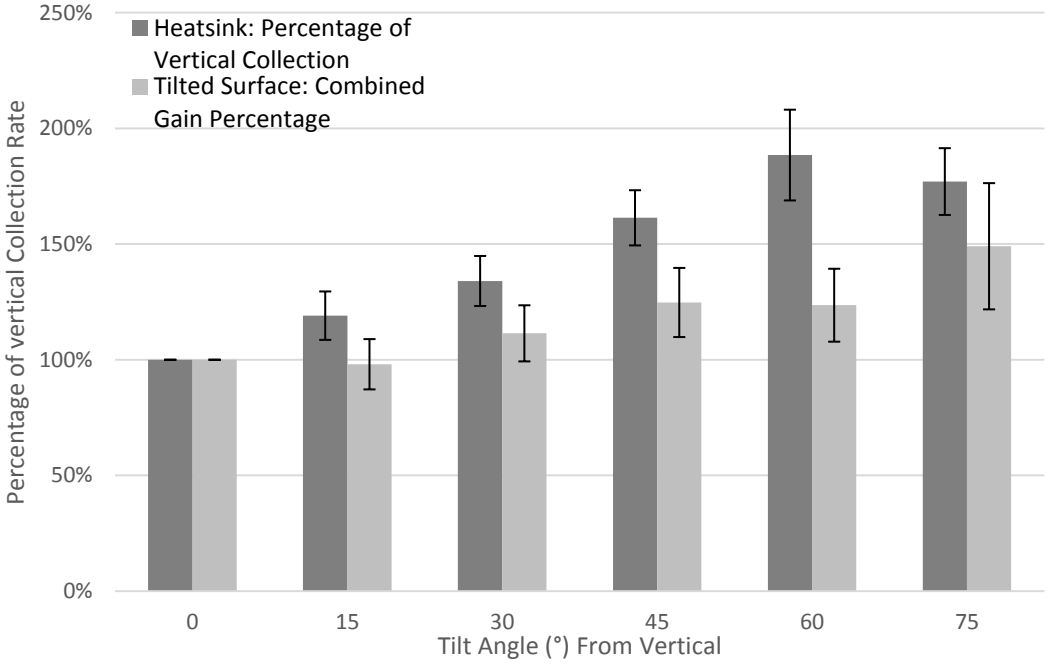

Figure 50. Percentage of vertical collection of the tilted heatsink and associated combined angles of the tilted surface experiments, from 0° to 75° from the vertical.

Figure 50 shows a separation, but similar trend, between the tilted heatsink and surface combination between 0° and 45°, which suggests that the surface combination is a reasonable approximation of the fin for these angles. However, at 60° there is a significant departure between the two. Note that 60° is also when significant condensate bridging between fins starts to occur in the tilted heatsink experiment. Given that the tilted surface experiment does not experience this effect at all, this might explain the departure shown at 60° in the above figure. At 75°, the departure is much less severe, possibly indicating that bridging is less effective at this angle. This seems to lend credence to the theory that some amount of bridging increases water collection rate presented in the tilted heatsink results.

Clearly the combined surface is not an excellent approximation of the heatsink fin. A possible reason for the discrepancy between the heatsink and surface combination values shown is that the heatsink fins share one source of heat transfer between both sides of the fin, while the combined surfaces each have one source. This means that for the combined surfaces, each side gets an equal amount of power, regardless of how effective each side is. On the other hand, the heatsink fin would inherently distribute more power to the more effective side, as more water collected is likely associated with more heat transfer in this case. It makes sense that distributing more power to the stronger, upward facing side would result in the more effective water collection shown by the heatsink in Figure 50 from 0° to 45°. Granted, this hypothesis would suggest that the gap between the two would be smaller at the lower angles, and grow as the angles grew larger, because the difference in power distribution is less important when the sides are nearer in effectiveness. This effect is not represented in the calculation shown by Figure 50.

4.3.6 Tilted Heatsink Timeline

The TEC prototype is set up in the same fashion as the normal fan-cooled test, but it is tilted with respect to the fan's axis by 75° (with vertical fins being 0°). This is done by holding the plastic base plate in a vise. Tests are performed with varying durations, from 1 to 9 hours in one hour increments. The purpose of this test is to determine the effect of collection duration on water collection rate for a tilted heatsink, specifically when bridging between fins is present. Longer tests result in more

developed bridging, so this experiment will help to isolate the effects of bridging. A 75° angle is used for this experiment because of the prominent bridging effect observed at this angle. An example of this set up with the 75° angle is shown below in Figure 51.

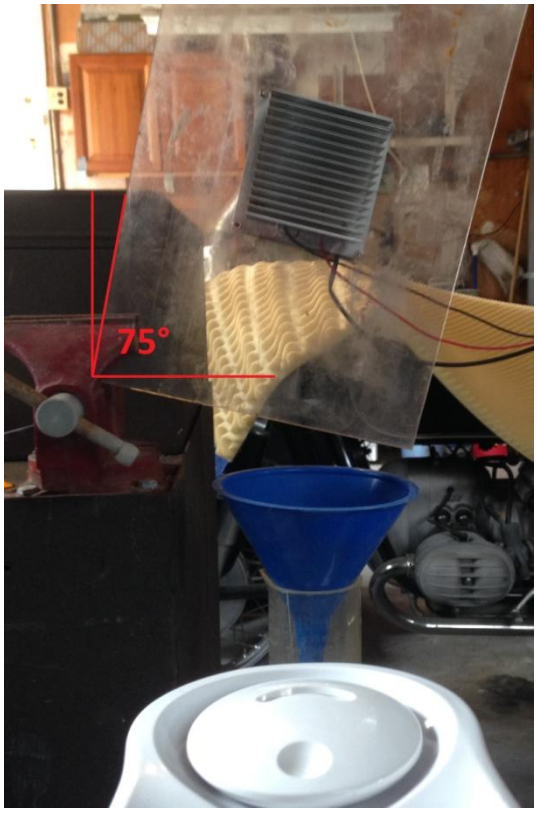

Figure 51. Tilted heatsink timeline experimental setup with 75° tilt.

Table 7 and Figure 52 show the results of this experiment.

Table 7. Average collection rates for 75° tilted heatsink sorted by total collection time from 1 to 9 hours.

Time (h)	Average L/kWh	Uncertainty (±)	Average kWh/m^3	Uncertainty (±)
1	0.104	0.016	9615	1439
2	0.125	0.016	8028	1003
3	0.120	0.016	8333	1081
4	0.156	0.016	6415	640
5	0.157	0.016	6388	635
6	0.148	0.016	6763	712
7	0.139	0.016	7171	800
8	0.142	0.016	7018	766
9	0.130	0.016	7698	922

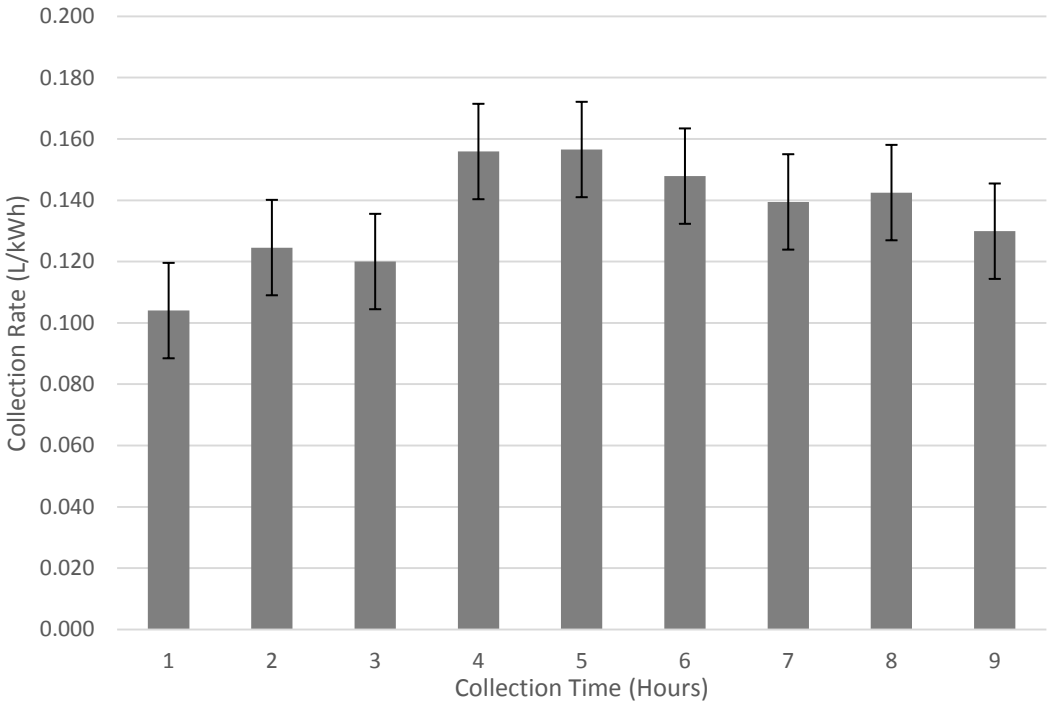

Figure 52. Average collection rates for 75° tilted heatsink sorted by total collection time from 1 to 9 hours.

Figure 52 shows a relatively low collection rate for 1-3 hour tests, a minor peak in the 4-5 hour range, and a steady drop off from 6-9 hours. There is some unexpected

variance for the 3 and 8 hour test durations, but this is due to environmental factors, and the window of uncertainty covers the expected average collection value. In previous experiments it was observed that a clear surface would collect water better than a wet one, but also that bridging might have a positive effect on water collection. It is possible that the former effect is prominent in the 1 and 2 hour tests, and the latter is prominent in the 4 and 5 hour tests. The dip observed for the 3 hour test may be because the 3 hour test doesn't benefit as much from either effect, but environmental variance may be just as likely. Figures 53-58 show the state of bridging at the 1-6 hour marks, respectively. Bridging after the 6 hour mark remained relatively unchanged.

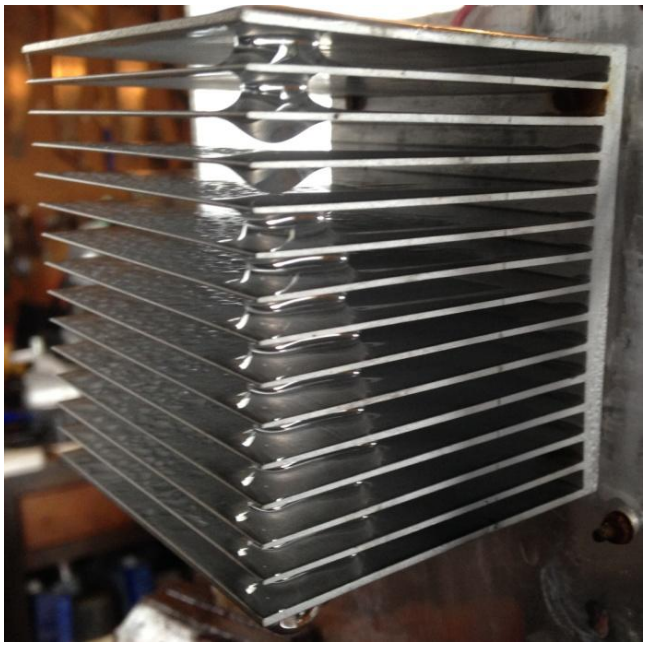

Figure 53. Tilted heatsink timeline condensate bridging at the 1 hour mark.

Figure 54. Tilted heatsink timeline condensate bridging at the 2 hour mark.

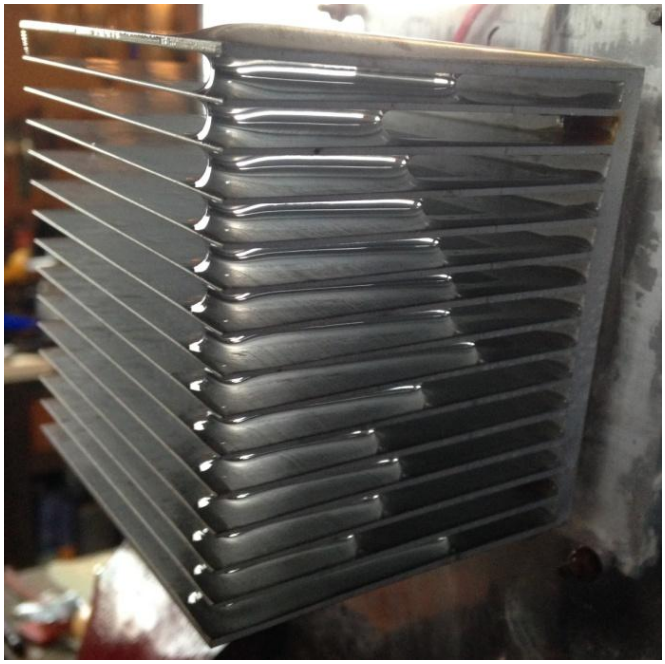

Figure 55. Tilted heatsink timeline condensate bridging at the 3 hour mark.

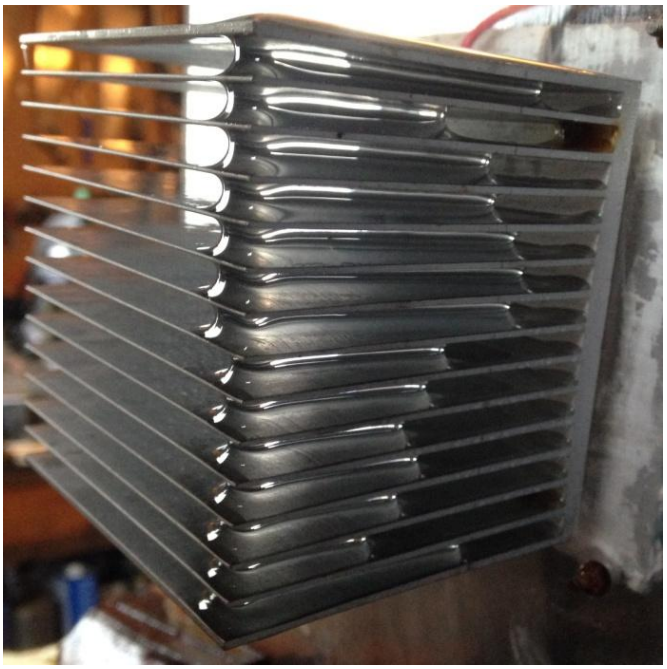

Figure 56. Tilted heatsink timeline condensate bridging at the 4 hour mark.

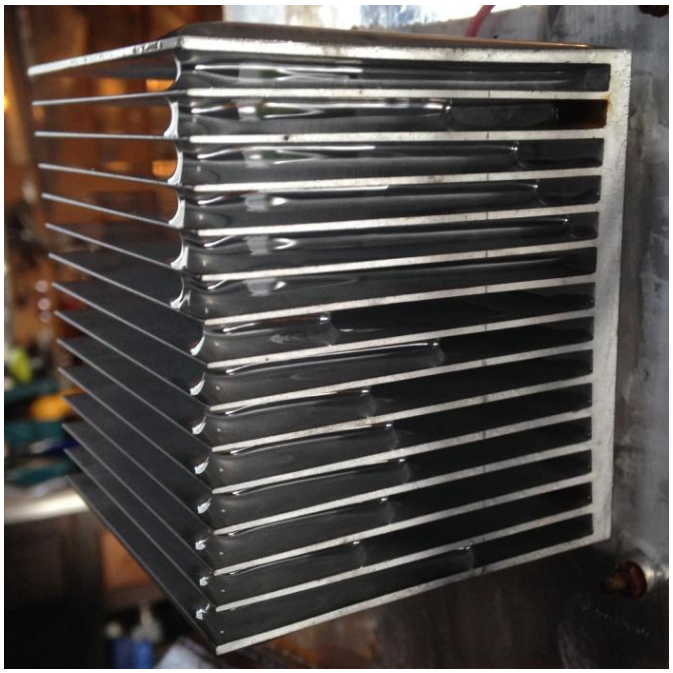

Figure 57. Tilted heatsink timeline condensate bridging at the 5 hour mark.

Figure 58. Tilted heatsink timeline condensate bridging at the 6 hour mark.

The amount of condensate bridging rapidly increases from 1-4 hours, and slowly tapers off to a fairly constant value after 6 hours. When considered with the collection data showing a maximum collection rate occurring at 4-5 hours, this suggests that the bridging may be most beneficial when just reaching the point at which its growth starts to slow.

Every time the heatsink is cleared of water prior to taking a measurement, some amount of water is left on the fins and the clearing tool (hex wrench). Assuming that the amount of water lost this way is a constant amount, this affects the shorter tests significantly more than the longer ones, as the amount lost is a greater percentage of the total amount collected. While including this effect is important when looking at overall efficiency, if the effect of bridging is to be isolated, it should be excluded. Table 8

and Figure 59 below show the data from Figure 53 if a constant 2mL of collected water is added to the average, an approximation of what is lost on the heatsink and hex wrench when clearing it.

Table 8. Average collection rates for 75° tilted heatsink sorted by total collection time from 1 to 9 hours with approximate 2mL clearing loss added into the average collection amount.

Time (h)	Average L/kWh	Uncertainty (±)	Average kWh/m^3	Uncertainty (±)
1	0.144	0.016	6944	772
2	0.145	0.016	6877	757
3	0.134	0.016	7469	893
4	0.166	0.016	6029	582
5	0.165	0.016	6077	591
6	0.155	0.016	6464	669
7	0.145	0.016	6890	760
8	0.148	0.016	6763	732
9	0.125	0.016	8018	1029

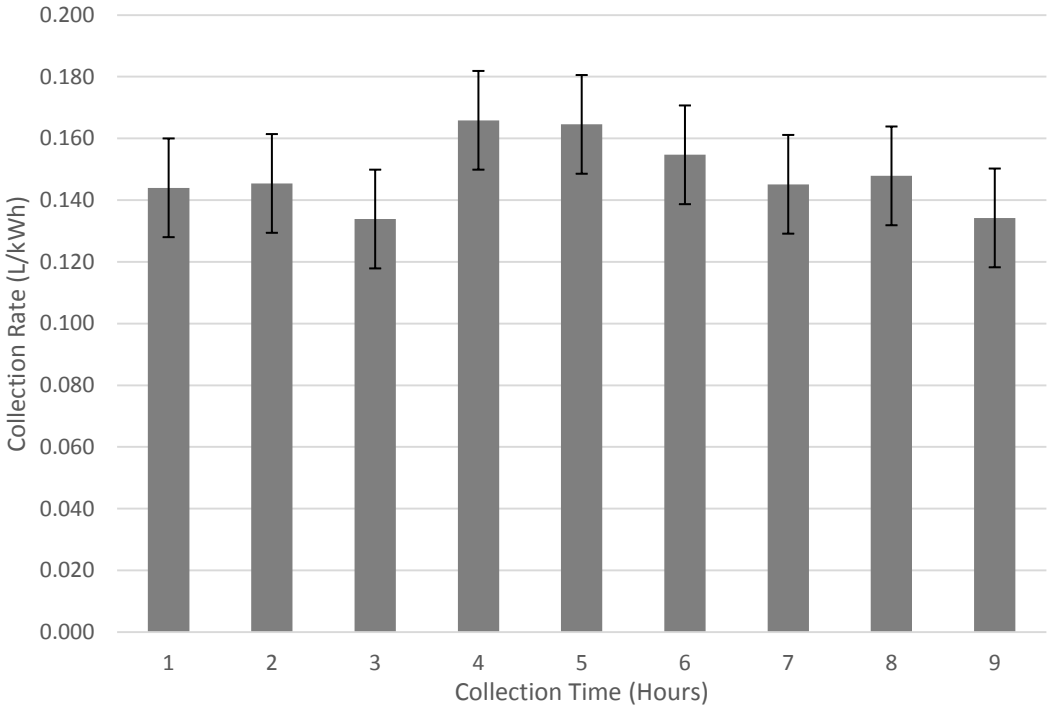

Figure 59. Average collection rates for 75° tilted heatsink sorted by total collection time from 1 to 9 hours with approximate 2mL clearing loss added into the average collection amount.

Figure 59 shows a much tighter spread of collection rates than in Figure 52, but the general trend stays the same. The tests at 1 and 2 hours come up significantly, but the peak still occurs at 4-5 hours, and the gradual drop off is still present. However, with this representation, it could be argued that the size of the condensate bridging that grows over the test duration has a relatively minor effect on the collection rate, especially given the uncertainty present.

4.4 Uncertainty

The uncertainty values used for all experiments and the devices used to measure each quantity are shown in Tables 9 and 10 below.

Table 9. Measured uncertainties and measuring devices for the vapor compression, TEC surface and water cooling experiments.

	RH (%)		T(°F)	H2O (ml)	H2O (L)	kWh	L/kWh
Symmetric Uncertainty	<90%	2.50%	1	5	0.005	0.005	Calc
	>90%	5.00%					
Measuring Device	Fluke 971 Temperature Humidity Reader			Graduated Cylinder		Kill A Watt EZ Watt Meter	

Table 10. Measured uncertainties and measuring devices for the TEC tilted heatsink, tilted surface, and tilted heatsink timeline experiments.

	Angle (°)	T (°F)	Ts (°F)	dT (°F)	H2O (ml)	H2O (L)	kWh	Time (h:m)	L/kWh
Symmetric Uncertainty	2	1.50%	1.50%	Calc	5	0.005	0.005	0:01	Calc
Measuring Device	Protractor and Level	Fluke 62 Max IR Thermometer			Graduated Cylinder		Kill A Watt EZ Watt Meter		

The majority of the uncertainties shown in Tables 9 and 10 are prescribed by the device manufacturer or by the resolution of the device reading. However, the uncertainties of the angle and water measurements have been adjusted slightly. The uncertainty of the angle measurement is raised to ±2°, despite the resolution of the protractor being 1°, because the addition of the level adds some uncertainty to the measurement. The uncertainty of the water measurement is set to ±5ml. This is the standard for a graduated cylinder with a resolution of 10ml, but the water level measurements in the experiment were taken as a difference of two measurements, which would result in higher uncertainty. However, the way the water runs down the

thread into the cylinder creates a very flat fluid surface, almost entirely without meniscus, which can be read more accurately than ±5ml. This is shown in Figure 60 below. Given the sharpness of the water line, it seems reasonable that it could be read to within 2.5ml, and that the total uncertainty could fall under ±5ml.

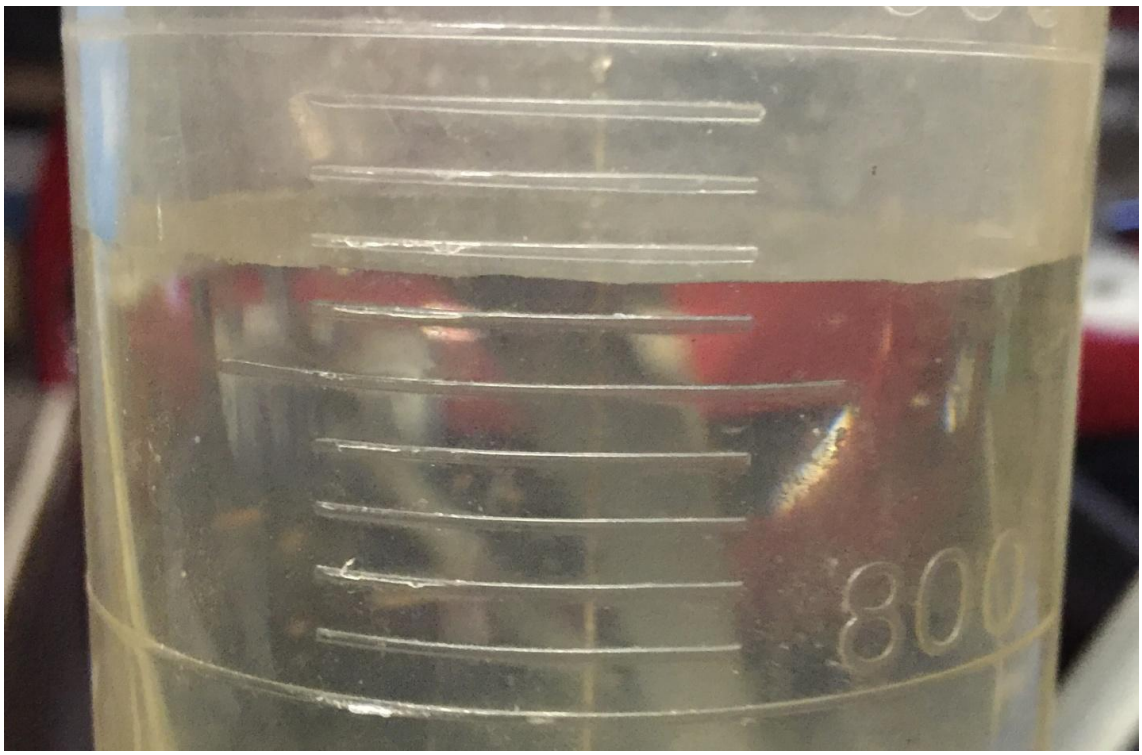

Figure 60. Graduated cylinder reading 866±2.5ml of water.

For all experiments, the random error far outweighed the instrumental error, and so the random error is what is reported and used in the error bars shown on the figures. This is likely due to the uncontrolled temperature and ambient humidity of the experiments, making each trial unique. Additionally, the error used for each angle trial in the relevant experiments is set to the largest random error for any angle trial of the entire experiment. This is a conservative measure based on the assumption that the

random error of any given trial could have been increased by including potentially more varied trials, up to a “worst case scenario,” which is this case is approximated by the experiment angle with the greatest random error. For example, in the tilted surface experiment, the error is set to ±0.012 L/kWh, which is the random error of the 30° trial average, but it is reasonable to assume that given more trials, this level of variance could have appeared in any of the other angle trials as well. This reflects the suspicion that if another angle in the experiment has a much lower random error, it may be due to a random occurrence of high precision, but not necessarily high accuracy.

Chapter 5: Conclusions and Recommendations

Concerning the economic viability of active atmospheric water collection, the results from these vapor-compression and TEC prototypes are unfavorable in the current form. The experiments show an approximate maximum collection rate of 1.25 L/kWh for the vapor compression prototype, and 0.318 L/kWh for the thermoelectric cooling prototype; well below other methods of fresh water collection, most notably the 315 L/kWh provided by reverse osmosis desalination. Even in the most favorable conditions, the collection rate from these prototypes is orders of magnitude lower than that of desalination or groundwater. Water collected by the vapor compression prototype is significantly more expensive than tap water, though it competes with bottled water. If space is not a concern, passive collection is likely a more viable alternative as well. However, these devices do not require the immense capital investment or infrastructure of desalination or ground water. This makes it uniquely suited for situations where the capital investments required or infrastructure of other methods are prohibitive. Some example situations include shorter required collection periods, such as emergency situations or times of drought; areas without access to plentiful ground water resources or direct access to the sea; or areas without the capital to invest in larger water collection endeavors.

While the TEC prototype's water collection rate efficiency is certainly poor in comparison to the vapor compression prototype, it does present some interesting results. The surfaces experiment shows that a Teflon coating can increase water collection by up to 29% from standard aluminum, and that clearing the surface can

improve collection by approximately 15%. The heatsink tilt experiment shows that a tilt angle of between 60-75° can increase water yield by up to 89% in certain conditions. The tilted surface experiment shows that this increase can likely be attributed to a combination of a more beneficial flow pattern, and a beneficial effect of condensate bridging between fins. The heatsink timeline experiment suggests that while the effect of bridging may be minor, that there is some optimal bridging state possible for a given geometry. These results suggest that for any given collection surface geometry (namely heatsinks) there is some optimal positioning, flow profile, and surface coating that will yield the most efficient performance. However, the effects of these parameters' extreme dependence on the geometry of the collection surface requires that similar experiments be performed on any new geometry in order to determine its unique optimal operating parameters. If these parameters were to be applied to a more efficient device, like an optimized vapor compression unit, the impact on performance could be significant.

The experimental setup and conditions for these experiments were limited by loosely controlled environmental conditions and limited resources, and some recommendations follow. A tightly controlled chamber to more accurately represented foggy conditions would greatly improve the accuracy of the experiment. Given that flow profile is such an important parameter, mimicking the flow profile of a fog bank as closely as possible would be ideal. Additionally, eliminating a lot of the environmental variability would go a long way towards reducing uncertainty and producing more accurate results. Using more powerful prototypes, or several in an array, would serve to

mitigate some of the uncertainty associated with collecting and measuring small quantities of water. This would also allow for much shorter experiment durations. In the case of the TEC prototype, it would also allow the TEC elements to be operated at a more efficient, lower power usage, and still collect enough water for accurate measurement and timely experiments. Gathering data using a data acquisition system throughout the experiment would give better insight into the time-dependent behavior of the experiment. In tandem with this, an accurate weight measurement device on the whole system would allow for measurement of the water collected on the collection surface without clearing it, giving a better idea of how much water the surface holds over time. Comparing collection rate to the amount of water contained on the collection surface in real time could provide a definitive answer to the benefits of water held by the condensation surface. This information would be very useful for determining the maximum efficiency operating point of a given prototype. Compiling the data from several operating points of several collection surfaces could provide insight into how best to apply these parameters to existing devices, or how to create new, more efficient devices.

References

1. Swain, D (2014, August 31) California's drought very unlikely to improve in the short term [Web log post]. Retrieved from http://www.weatherwest.com/archives/1756
2. Cooley, Heather, Peter H. Gleick, and Gary Hartman. Wolff. Desalination, with a Grain of Salt: A California Perspective. Oakland, CA: Pacific Institute for Studies in Development, Environment, and Security, 2006. Waterboards.com. Web. Retrieved from http://www.waterboards.ca.gov/water_issues/programs/grants_loans/water_recycling/docs/econ_tskfrce/25.pdf
3. Visser, Klaas. Waste Heat Recovery For Desalination From Steam Power Plants. Wateronline.com. web. Retrieved from https://www.wateronline.com/doc/waste-heat-recovery-for-desalination-from-steam-power-plants-0001
4. KSB AG. (n.d.). Seawater desalination system. Retrieved from https://www.ksb.com/centrifugal-pump-lexicon/seawater-desalination-system/191728/
5. Reverse Osmosis Desalination System. (2018, February 27). Retrieved from http://www.windies-online.com/reverse-osmosis-desalination-system/907
6. "Electric Power Monthly by State." EIA. U.S. Energy Information Administration, Aug. 2014. Web. 14 Sept. 2014. http://www.eia.gov/electricity/monthly/epm_table_grapher.cfm?t=epmt_5_6_a
7. Rogers, P (2014, May 29) Nation's largest ocean desalination plant goes up near San Diego. San Jose Mercury News. Retrieved from http://www.mercurynews.com/science/ci_25859513/nations-largest-ocean-desalination- plant-goes-up-near
8. Park, Kyoo-Chul, Shreerang S. Chhatre, Siddarth Srinivasan, Robert E. Cohen, and Gareth H. McKinley. Optimal Design of Permeable Fiber Network Structures for Fog Harvesting. Tech. Washington, DC: ACS, 2013. Web.
9. Air HES - Clean water and energy from clouds. VCstart. (2014). Retrieved from https://vcstart.com/en/project/air-hes-clean-water-and-energy-from-clouds
10. "Eole Water - Making Water from Air." Eole Water - Give Us Wind, We Give You Water | Our Expertise. N.p., n.d. Web. Retrieved from http://www.eolewater.com/gb/our-products/our-expertise.html
11. Frey, Thomas. A Study of Future Trends and Predictions. FuturistSpeaker.com A Study of Future Trends and Predictions by Futurist Thomas Frey RSS. N.p., 8 Sept. 2013. Web. Retrieved from

http://www.futuristspeaker.com/2013/09/tapping-into-the-waterways-in-the-sky/
12. How Does A Dehumidifier Work? AchooAllergy. (2014). Retrieved from http://www.achooallergy.com/how-does-a-dehumidifier-work.asp
13. Desiccant Dehumidifiers: Functional Principle and technical Differences. Trotec. (2018). Retrieved from https://uk.trotec.com/products/machinery-homecomfort/dehumidification/practical-knowledge-concerning-dehumidifiers/overview-of-dehumidification-methods/desiccant-dehumidifiers/
14. EDV-2200 mid Size Dehumidifier. Eva-dry.com. Retrieved from https://www.eva-dry.com/eva-dry-2200-electric-dehumidifier
15. Brown, D. R.; N. Fernandez; J. A. Dirks; T. B. Stout (March 2010). The Prospects of Alternatives to Vapor Compression Technology for Space Cooling and Food Refrigeration Applications. Pacific Northwest National Laboratory (PNL). U.S. Department of Energy. Retrieved from https://www.pnnl.gov/main/publications/external/technical_reports/pnnl-19259.pdf
16. Introduction to Thermoelectric Coolers. Tec Microsystems. Retrieved from http://www.tec-microsystems.com/EN/Intro_Thermoelectric_Coolers.html
17. Technology Principle. FrozenTEC Thermoelectric Solutions. Retrieved from http://www.frozentec.com/technology-principal.html
18. Ken Brazier. A Diagram of a Thermoelectric Cooler. Wikipedia. Retrieved from https://en.wikipedia.org/wiki/Thermoelectric_effect#/media/File:Thermoelectric_Cooler_Diagram.svg
19. Asadnejad, A. (2011, October 07). Thermoelectric cooling, peltier cold plates, thermoelectric plates, direct contact cooling, heating, heat sinks, exchangers, Peltier coolers, devices - TECA Corporation. Retrieved from https://www.thermoelectric.com/2010/pr/cp/basic/aircooled.htm
20. Control System for a thermoelectric cooler. Olin NASA research group. Retrieved from http://nasa.olin.edu/projects/2011/tec/?page=software
21. Fog Types. National Weather Service Weather Forecast Office. (2014). Retrieved from http://www.crh.noaa.gov/jkl/?n=fog_types
22. Chapter 4: Fog. Environment Canada. (2014). Retrieved from http://www.ec.gc.ca/meteo-weather/default.asp?lang=En&n=279AC7ED-1&offset=4&toc=hide

23. Radiation Fog Formation. Experimental Aircraft Info. (2014). Retrieved from http://www.experimentalaircraft.info/wx/weather-fog.php
24. Rose, J. W. (2011, February 10) Dropwise Condensation. Thermopedia. Retrieved from http://www.thermopedia.com/content/708/
25. Basics of condensation. Thermal-Fluids Central. (2010, July 17). Retrieved from https://www.thermalfluidscentral.org/encyclopedia/index.php/Basics_of_condensation
26. Depew, C. A., Reisbig, R. L. Vapor Condensation on a Horizontal Tube Using Teflon to Promote Dropwise Condensation. (1964, October). Retrieved from http://pubs.acs.org/doi/pdf/10.1021/i260012a017
27. Drying Your Compressed Air System Will Save Real Money. Maintenance World. (2014). retrieved from http://www.maintenanceworld.com/wp-content/uploads/2013/07/graph1.jpg

Appendix A

Raw Data Tables

Table A1. Vapor compression prototype high humidity steady state test data.

	Relative Humidity (%)	Temperature (°F)	Flowrate (m^3/s)	H2O (ml)	kWh (SS)	L/kWh (SS)	kWh/m^3 (SS)
Single Pulsed	98%	55	0.073	170	0.15	1.13	882
	100%	55	0.073	210	0.19	1.11	905
	100%	55	0.073	170	0.15	1.13	882
	100%	55	0.073	190	0.15	1.27	789
	100%	45	0.080	120	0.10	1.20	833
	88%	60	0.073	230	0.19	1.21	826
	88%	60	0.073	200	0.18	1.11	900
	88%	60	0.073	190	0.16	1.19	842
	88%	60	0.073	180	0.17	1.06	944
	90%	58	0.050	170	0.16	1.06	941
	90%	58	0.050	170	0.17	1.00	1000
	90%	58	0.050	180	0.16	1.13	889
	90%	58	0.050	150	0.14	1.07	933
	90%	58	0.050	190	0.16	1.19	842
	95%	61	0.061	155	0.14	1.11	903
	94%	58	0.061	170	0.15	1.13	882
	94%	58	0.061	135	0.12	1.13	889
	94%	58	0.061	170	0.15	1.13	882
	98%	56	0.061	215	0.18	1.19	837
	98%	56	0.061	186	0.16	1.16	860
	98%	56	0.061	204	0.18	1.13	882
	98%	56	0.061	150	0.13	1.15	867
	98%	56	0.061	260	0.22	1.18	846
Single Unpulsed	88%	46	0.073	250	0.26	0.96	1040
	100%	47	0.073	260	0.29	0.90	1115
	100%	52	0.091	100	0.10	1.00	1000
	100%	52	0.091	220	0.20	1.10	909
	100%	52	0.091	130	0.13	1.00	1000
	100%	51	0.091	130	0.15	0.87	1154
	100%	51	0.091	255	0.23	1.11	902
	100%	51	0.080	235	0.22	1.07	936
	100%	51	0.080	110	0.10	1.10	909
	100%	51	0.073	160	0.16	1.00	1000

	100%	51	0.073	250	0.23	1.09	920
	100%	51	0.073	180	0.18	1.00	1000
	97%	51	0.061	205	0.25	0.82	1220
	97%	51	0.061	115	0.14	0.82	1217
	97%	51	0.061	260	0.27	0.96	1038
	97%	53	0.061	70	0.06	1.17	857
	97%	53	0.061	260	0.23	1.13	885
	85%	55	0.061	220	0.26	0.85	1182
	98%	55	0.073	170	0.15	1.13	882

Table A2. Surfaces test data.

Aluminum Plate	RH (%)	T(°F)	H2O (ml)	kWh	L/kWh	Avg L/kWh	Avg kWh/m^3
No Clear	58%	71	30	0.40	0.020		
	62%	62	15	0.19	0.021		
	48%	67	20	0.39	0.014		
	65%	67	20	0.38	0.014		
	66%	63	25	0.47	0.014		
	44%	74	20	0.51	0.010	0.015	64843
Clear	80%	55	20	0.19	0.028		
	50%	60	20	0.40	0.013		
	60%	62	15	0.45	0.009		
	60%	64	40	0.41	0.026		
	80%	60	32	0.49	0.017		
	35%	67	20	0.42	0.013	0.018	56912
Pan	RH (%)	T(°F)	H2O (ml)	kWh	L/kWh	Avg L/kWh	Avg kWh/m^3
No Clear	49%	70	30	0.40	0.020		
	48%	68	20	0.55	0.010		
	53%	67	40	0.37	0.029		
	57%	63	20	0.27	0.020		
	49%	70	30	0.31	0.026		
	50%	69	20	0.55	0.010		
	53%	67	40	0.37	0.029		
	57%	63	20	0.27	0.020		
	62%	68	30	0.31	0.026		
	65%	64	23	0.37	0.016		
	50%	73	30	0.39	0.020		
	69%	64	40	0.47	0.022		
	67%	72	20	0.35	0.015		

	80%	65	35	0.39	0.024		
	66%	65	25	0.45	0.015		
	91%	52	50	0.70	0.019		
	59%	71	30	0.55	0.014	0.020	51144
	74%	64	20	0.30	0.018		
	80%	65	30	0.30	0.026		
Clear	81%	65	25	0.28	0.024		
	83%	62	30	0.36	0.022		
	74%	59	35	0.37	0.025	0.023	43623
Fanned plate	RH (%)	T(°F)	H2O (ml)	kWh	L/kWh	Avg L/kWh	Avg kWh/m^3
	65%	52	32	0.49	0.017		
	51%	77	31	0.38	0.022		
	58%	67	40	0.32	0.033		
No clear	50%	78	39	0.48	0.021		
	48%	74	56	0.35	0.042		
	56%	64	45	0.31	0.038		
	32%	82	50	0.80	0.017		
	40%	75	20	0.20	0.026	0.027	36895
Heatsink	RH (%)	T(°F)	H2O (ml)	kWh	L/kWh	Avg L/kWh	Avg kWh/m^3
	55%	62	77	0.60	0.034		
	36%	76	45	0.45	0.026		
	61%	61	81	0.69	0.031		
No Clear	35%	78	32	0.29	0.029		
	41%	75	39	0.27	0.038		
	53%	66	31	0.26	0.031		
	56%	63	31	0.22	0.037	0.032	30788

Table A3. Water cooling test data.

Pan	RH (%)	T(°F)	T(°C)	Ts(°F)	Ts(°C)	dT(°F)	dT(°C)	H2O (ml)	kWh	L/kWh	Avg L/kWh	Avg kWh/m^3	Avg dT(°C)
Water Cooled	48%	70	21.1	54	12.2	16	8.9	12	0.23	0.052			
	63%	64	17.8	52	11.1	12	6.7	35	0.28	0.125			
	57%	66	18.9	53	11.7	13	7.2	20	0.20	0.100			
	46%	75	23.9	63	17.2	12	6.7	40	0.34	0.118			
	60%	65	18.3	52	11.1	13	7.2	23	0.14	0.164			
	55%	69	20.6	58	14.4	11	6.1	25	0.23	0.109			
	50%	75	23.9	50	10.0	25	13.9	21	0.22	0.095	0.109	9171	8.1
Fan Cooled	52%	80	26.7	72	22.2	8	4.4	7	0.18	0.039			
	61%	63	17.2	55	12.8	8	4.4	10	0.14	0.071			
	64%	64	17.8	55	12.8	9	5.0	17	0.28	0.061			
	66%	64	17.8	58	14.4	6	3.3	16	0.29	0.055			
	63%	63	17.2	54	12.2	9	5.0	32	0.55	0.058			
	62%	62	16.7	53	11.7	9	5.0	20	0.44	0.045			
	58%	66	18.9	56	13.3	10	5.6	9	0.16	0.056	0.055	18130	4.7

Table A4. Tilted heatsink split flow test data.

Angle	T(F)	Ts(F)	dT	H2O (ml)	kWh	Time	L/kWh	Avg L/kWh	Avg kWh/m^3
0	73	58	15	112	0.69	7:38	0.162		
0	76	60	16	85	0.70	8:00	0.121		
0	70	57	13	40	0.34	3:56	0.118		
0	73	58	15	105	0.83	9:26	0.127	0.132	7577
15	72	58	14	110	0.70	8:01	0.157	0.157	6364
30	81	62	19	138	0.78	8:54	0.177	0.177	5652
45	76	58	18	181	0.85	9:42	0.213		
45	73	59	14	152	0.72	8:17	0.211		
45	72	61	11	275	1.28	14:27	0.215	0.213	4696
60	75	58	17	159	0.72	8:16	0.221		
60	75	59	16	176	0.72	8:18	0.244		
60	76	63	13	340	1.21	13:55	0.281	0.249	4020
75	71	58	13	180	0.81	9:06	0.222		
75	75	61	14	240	1.04	11:51	0.231		
75	75	61	14	300	1.21	13:49	0.248	0.234	4280
90 (9 Hr)	70	53	17	160	0.79	8:54	0.203	0.203	4938
90 (24 Hr)	75	55	20	264	2.08	23:49	0.127	0.127	7879

Table A5. Tilted heatsink through flow test data.

Angle	T(F)	Ts(F)	dT	H2O (ml)	kWh	Time	L/kWh	kWh/m^3
0	71	62	9	140	1.04	11:52	0.135	7429
15	68	59	9	170	1.10	12:27	0.155	6471
30	70	60	10	205	1.14	12:45	0.180	5561
45	70	60	10	205	1.05	11:49	0.195	5122
60	69	59	10	265	1.26	14:07	0.210	4755
75	69	61	8	270	1.22	13:46	0.221	4519
90 (12 Hr)	68	54	14	170	1.07	11:56	0.159	6294
90 (24 Hr)	75	59	16	275	2.12	24:26	0.130	7709

Table A6. Tilted surface test data.

Angle	T(F)	Ts(F)	dT	H2O (ml)	kWh	Time	L/kWh	Avg L/kWh	Avg kWh/m^3
15	72	60	12	210	0.63	11:03	0.333		
15	68	58	10	215	0.65	11:30	0.331		
15	70	60	10	200	0.68	12:00	0.294		
15	67	57	10	210	0.66	11:49	0.318	0.319	3134
30	60	50	10	130	0.65	10:11	0.200		
30	58	49	9	180	0.76	11:46	0.237		
30	60	51	9	200	0.73	11:12	0.274		
30	56	45	11	150	0.61	9:33	0.246		
30	55	45	10	120	0.59	8:56	0.203		
30	57	49	8	140	0.79	11:58	0.177		
30	59	50	9	215	0.80	12:11	0.269		
30	62	53	9	220	0.78	12:02	0.282		
30	56	48	8	150	0.65	9:53	0.231		
30	56	46	10	240	0.90	13:26	0.267	0.239	4192
45	61	52	9	185	0.73	10:56	0.253		
45	57	48	9	132	0.58	8:41	0.228		
45	60	51	9	130	0.62	9:26	0.210		
45	57	48	9	165	0.71	10:54	0.232		
45	59	52	7	150	0.79	12:00	0.190		
45	59	50	9	120	0.59	9:17	0.203	0.213	4704
60	62	52	10	125	0.69	10:30	0.181		
60	62	53	9	138	0.66	9:46	0.209		
60	61	51	10	135	0.82	12:24	0.165		
60	60	50	10	115	0.70	10:26	0.164	0.180	5562
75	59	50	9	105	0.71	10:47	0.148		

75	59	49	10	80	0.69	10:25	0.116		
75	57	50	7	87	0.63	9:47	0.138		
75	59	49	10	88	0.57	10:40	0.154		
75	57	48	9	90	0.72	11:07	0.125	0.136	7339
90	68	56	12	90	0.82	10:57	0.110		
90	71	58	13	105	0.79	10:48	0.133		
90	69	57	12	95	0.72	9:55	0.132		
90	62	52	10	103	0.81	12:06	0.127	0.125	7972
105	64	52	12	90	0.74	11:48	0.122		
105	63	52	11	70	0.62	10:12	0.113		
105	64	53	11	62	0.64	10:54	0.097		
105	62	51	11	70	0.65	10:58	0.108	0.110	9110
120	64	53	11	68	0.65	11:00	0.105		
120	71	60	11	65	0.66	11:45	0.098		
120	76	65	11	58	0.57	10:16	0.102		
120	73	62	11	65	0.69	13:14	0.094	0.100	10024
135	67	57	10	105	0.75	10:56	0.140		
135	65	55	10	90	0.71	10:23	0.127		
135	66	56	10	100	0.87	12:44	0.115		
135	65	56	9	100	0.76	11:11	0.132		
135	65	54	11	85	0.69	10:15	0.123		
135	63	50	13	45	0.66	9:28	0.068		
135	60	49	11	60	0.71	10:15	0.085		
135	62	52	10	52	0.68	10:00	0.076		
135	63	54	9	75	0.68	10:09	0.110		
135	63	50	13	45	0.66	9:28	0.068		
135	60	49	11	60	0.71	10:15	0.085		
135	62	52	10	52	0.68	10:00	0.076	0.100	9958

150	54	46	8	40	0.59	9:03	0.068		
150	56	46	10	40	0.60	9:15	0.067		
150	53	45	8	55	0.85	13:07	0.065		
150	54	47	7	60	0.85	13:12	0.071		
150	51	45	6	70	0.84	12:27	0.083		
150	51	44	7	65	0.91	13:51	0.071		
150	51	44	7	65	0.84	13:20	0.077		
150	53	45	8	60	0.77	11:56	0.078		
150	53	44	9	55	0.79	12:36	0.070		
150	56	46	10	55	0.84	13:02	0.065	0.071	13988
165	58	51	7	35	0.73	11:44	0.048		
165	59	51	8	55	0.64	10:31	0.086		
165	60	53	7	40	0.75	12:00	0.053		
165	60	52	8	43	0.83	13:08	0.052		
165	60	52	8	20	0.71	11:20	0.028		
165	60	52	8	30	0.71	11:15	0.042		
165	62	52	10	35	0.66	10:40	0.053		
165	62	52	10	45	0.75	12:02	0.060		
165	58	51	7	50	0.78	12:24	0.064		
165	56	48	8	58	0.93	14:52	0.062	0.055	18217

Table A7. Heatsink and combined tilted surface percentage of vertical collection data.

Angle(°)	Tilted Heatsink		Tilted Surface Combined	
	Percentage of Vertical Collection	Uncertainty(±)	Percentage of Vertical Collection	Uncertainty(±)
0	100%	0%	100%	0%
15	119%	10%	98%	11%
30	134%	11%	111%	12%
45	161%	12%	125%	15%
60	188%	20%	124%	16%
75	177%	14%	149%	27%

Table A8. Heatsink timeline test data.

Angle	T(F)	Ts(F)	dT	H2O (ml)	kWh	Time(hours)	L/kWh	Avg L/kWh	Avg kWh/m3
75	73	63	10	4	0.05	1	0.080		
75	55	49	6	5	0.05	1	0.100		
75	57	52	5	5	0.05	1	0.100		
75	59	52	7	7	0.05	1	0.140		
75	57	52	5	5	0.05	1	0.100	0.104	9615
75	74	63	11	18	0.11	2	0.164		
75	66	55	11	12	0.11	2	0.109		
75	80	64	16	10	0.10	2	0.100		
75	76	66	10	13	0.10	2	0.130		
75	65	59	6	15	0.10	2	0.150		
75	66	58	8	15	0.10	2	0.150		
75	64	58	6	13	0.10	2	0.130		
75	56	50	6	5	0.10	2	0.050		
75	59	52	7	18	0.10	2	0.180		
75	59	52	7	12	0.09	2	0.133		
75	61	55	6	5	0.09	2	0.056		
75	59	53	6	8	0.09	2	0.089		
75	60	54	6	10	0.09	2	0.111		
75	58	53	5	10	0.09	2	0.111		
75	59	52	7	15	0.09	2	0.167		
75	61	54	7	10	0.09	2	0.111		
75	56	48	8	8	0.09	2	0.089	0.125	8028
75	71	61	10	26	0.17	3	0.153		
75	74	63	11	15	0.15	3	0.100		
75	80	64	16	15	0.15	3	0.100		
75	75	61	14	12	0.15	3	0.080		

75	68	60	8	32	0.15	3	0.213		
75	61	55	6	20	0.15	3	0.133		
75	65	55	10	15	0.15	3	0.100		
75	64	58	6	15	0.14	3	0.107		
75	63	53	10	15	0.14	3	0.107		
75	57	50	7	20	0.13	3	0.154		
75	60	52	8	10	0.13	3	0.077		
75	64	56	8	15	0.13	3	0.115	0.120	8333
75	71	61	10	25	0.22	4	0.114		
75	76	65	11	30	0.20	4	0.150		
75	73	65	8	34	0.21	4	0.162		
75	75	64	11	25	0.18	4	0.139		
75	66	58	8	40	0.20	4	0.200		
75	60	59	1	40	0.20	4	0.200		
75	61	58	3	35	0.21	4	0.167		
75	63	59	4	35	0.21	4	0.167		
75	65	61	4	30	0.20	4	0.150		
75	59	51	8	20	0.18	4	0.111	0.156	6415
75	73	62	11	38	0.25	5	0.152		
75	63	58	5	50	0.25	5	0.200		
75	59	52	7	30	0.24	5	0.125		
75	63	60	3	50	0.25	5	0.200		
75	60	55	5	30	0.26	5	0.115		
75	59	54	5	35	0.25	5	0.140		
75	56	51	5	40	0.25	5	0.160		
75	55	52	3	40	0.25	5	0.160	0.157	6388
75	76	60	16	20	0.30	6	0.067		
75	82	68	14	42	0.30	6	0.140		
75	67	59	8	53	0.30	6	0.177		

75	56	51	5	45	0.25	6	0.180		
75	64	58	6	55	0.30	6	0.183		
75	60	58	2	55	0.32	6	0.172		
75	55	50	5	40	0.30	6	0.133		
75	61	55	6	25	0.30	6	0.083		
75	58	52	6	45	0.30	6	0.150		
75	65	55	10	35	0.30	6	0.117		
75	61	54	7	45	0.29	6	0.155		
75	65	59	6	50	0.30	6	0.167		
75	62	56	6	35	0.29	6	0.121		
75	63	55	8	35	0.29	6	0.121		
75	66	57	9	30	0.28	6	0.107	0.148	6763
75	65	53	12	40	0.40	7	0.100		
75	68	58	10	65	0.36	7	0.181		
75	65	57	8	55	0.35	7	0.157		
75	66	58	8	40	0.34	7	0.118		
75	60	53	7	60	0.35	7	0.171		
75	56	51	5	50	0.34	7	0.147		
75	59	55	4	60	0.37	7	0.162		
75	67	58	9	50	0.35	7	0.143		
75	70	60	10	35	0.35	7	0.100		
75	55	49	6	37	0.32	7	0.116	0.139	7171
75	58	52	6	55	0.37	8	0.149		
75	54	50	4	60	0.37	8	0.162		
75	52	49	3	55	0.37	8	0.149		
75	60	53	7	42	0.38	8	0.111	0.142	7018
75	69	59	10	82	0.49	9	0.167		
75	62	54	8	68	0.43	9	0.158		
75	68	56	12	45	0.49	9	0.092		

75	57	49	8	45	0.44	9	0.102	0.130	7698
75	57	51	6	65	0.48	10	0.135		
75	62	52	10	55	0.53	11	0.104		
75	60	56	4	110	0.62	12	0.177		

*Note: Highlighted trials are omitted as outliers.